Article

Cell Metabolism

Podoplanin-Expressing Macrophages Promote Lymphangiogenesis and Lymphoinvasion in Breast Cancer

Graphical Abstract

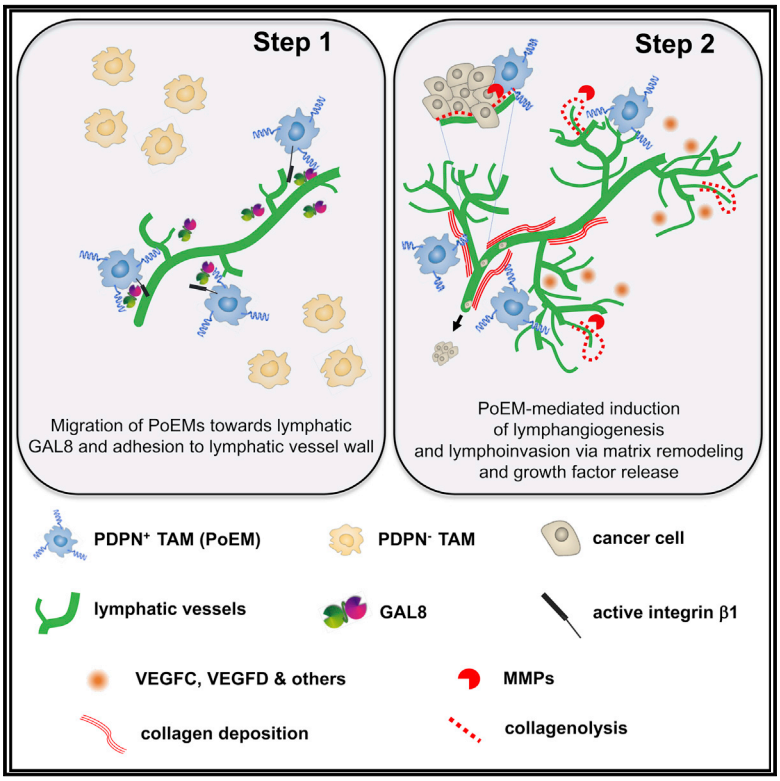

Authors

Paweł Bieniasz-Krzywiec, Rosa Martín-Pérez, Manuel Ehling, ..., Giuseppe Floris, Jo A. Van Ginderachter, Massimiliano Mazzone

Correspondence

massimiliano.mazzone@kuleuven.vib.be

In Brief

Bieniasz-Krzywiec et al. demonstrate a triad interaction of podoplanin (PDPN)-expressing tumor-associated macrophages (PoEMs), GAL8-expressing lymphatic vessels, and invading breast cancer cells, which promotes metastasis. PoEMs remodel the extracellular matrix, stimulating lymphangiogenesis, and release previously trapped cancer-promoting factors that facilitate cancer cell lymphoinvasion.

Highlights

- PoEMs, PDPN-expressing macrophages, localize in the proximity to tumor lymphatics
- PDPN activates β1 integrin, mediating PoEM binding to GAL8-expressing lymphatics
- PDPN in PoEMs promotes extracellular matrix remodeling
- *Pdpn* deletion in macrophages reduces breast tumor lymphangiogenesis and lymphoinvasion

Bieniasz-Krzywiec et al., 2019, Cell Metabolism *30*, 1–20
November 5, 2019
https://doi.org/10.1016/j.cmet.2019.07.015

CellPress

Please cite this article in press as: Bieniasz-Krzywiec et al., Podoplanin-Expressing Macrophages Promote Lymphangiogenesis and Lymphoinvasion in Breast Cancer, Cell Metabolism (2019), https://doi.org/10.1016/j.cmet.2019.07.015

Cell Metabolism
Article

Podoplanin-Expressing Macrophages Promote Lymphangiogenesis and Lymphoinvasion in Breast Cancer

Paweł Bieniasz-Krzywiec,[1,2,3,4] Rosa Martín-Pérez,[1,2] Manuel Ehling,[1,2] Melissa García-Caballero,[5] Sotiria Pinioti,[1,2] Samantha Pretto,[1,2] Roel Kroes,[1,2] Chiara Aldeni,[1,2] Mario Di Matteo,[1,2] Hans Prenen,[2,6] María Virginia Tribulatti,[7] Oscar Campetella,[7] Ann Smeets,[8] Agnes Noel,[5] Giuseppe Floris,[9] Jo A. Van Ginderachter,[3,4] and Massimiliano Mazzone[1,2,10,*]

[1]Laboratory of Tumor Inflammation and Angiogenesis, Center for Cancer Biology, VIB, Leuven B3000, Belgium
[2]Laboratory of Tumor Inflammation and Angiogenesis, Center for Cancer Biology, Department of Oncology, KU Leuven, Leuven B3000, Belgium
[3]Myeloid Cell Immunology Laboratory, VIB Center for Inflammation Research, Brussels B1050, Belgium
[4]Laboratory of Cellular and Molecular Immunology, Vrije Universiteit Brussel, Brussels B1050, Belgium
[5]Laboratory of Tumor and Developmental Biology, GIGA-Cancer, University of Liège, Sart-Tilman, B4000 Liège, Belgium
[6]Oncology Department, University Hospital Antwerp, 2650 Edegem, Belgium
[7]Institute for Research in Biotechnology, National University of San Martín, CONICET, Buenos Aires 1650, Argentina
[8]Surgical Oncology Unit, Department of Oncology, KU Leuven, Leuven B3000, Belgium
[9]Translational Cell and Tissue Research Unit, Department of Imaging and Pathology, KU Leuven, Leuven B3000, Belgium
[10]Lead Contact
*Correspondence: massimiliano.mazzone@kuleuven.vib.be
https://doi.org/10.1016/j.cmet.2019.07.015

SUMMARY

Among mammary tumor-infiltrating immune cells, the highest expression of podoplanin (PDPN) is found in a subset of tumor-associated macrophages (TAMs). We hereby demonstrate that PDPN is involved in the attachment of this TAM subset to lymphatic endothelial cells (LECs). Mechanistically, the binding of PDPN to LEC-derived galectin 8 (GAL8) in a glycosylation-dependent manner promotes the activation of pro-migratory integrin β1. When proximal to lymphatics, PDPN-expressing macrophages (PoEMs) stimulate local matrix remodeling and promote vessel growth and lymphoinvasion. Anti-integrin β1 blockade, macrophage-specific *Pdpn* knockout, or GAL8 inhibition impairs TAM adhesion to LECs, restraining lymphangiogenesis and reducing lymphatic cancer spread. In breast cancer patients, association of PoEMs with tumor lymphatic vessels correlates with incidences of lymph node and distant organ metastasis.

INTRODUCTION

Despite the numerous advances that have been achieved in the treatment of breast cancer, the prognosis for patients with a metastatic disease remains poor, with a median survival of 2–4 years (Ayoub et al., 2012). Regional lymph nodes (LNs) are the primary sites of lymphatic drainage from all areas of the breast, and the extent of their involvement in breast cancer is a strong predictor of disease relapse and patient survival. Migration of cancer cells into the lymphatic circulation and entry into the LNs is greatly facilitated by tumor lymphangiogenesis, a process that generates new lymphatic vessels (LVs) from pre-existing conduits (Ran et al., 2010; Skobe et al., 2001). Clinical studies have shown that the production of lymphangiogenic factors and the

Context and Significance

Migration of cancer cells into the lymph accelerates cancer spreading (metastasis). Immune cells, in particular macrophages, play critical roles in cancer, and tumor-associated macrophages (TAMs) have been shown to promote the formation of new lymph vessels. Researchers at the VIB-KU Leuven Center for Cancer Biology in Belgium show that a TAM subset expresses a molecule called podoplanin (PDPN), which specifically interacts with a lymphatic vessel molecule (galectin 8) to promote new lymph vessel formation and the migration of cancer cells through the lymphatic system. Experimental removal of PDPN-expressing macrophages (PoEMs) or inhibition of galectin 8 decreases cancer metastasis in mouse breast cancer models. The investigators also provide proof of concept of PoEMs as a potential prognostic marker in breast cancer patients.

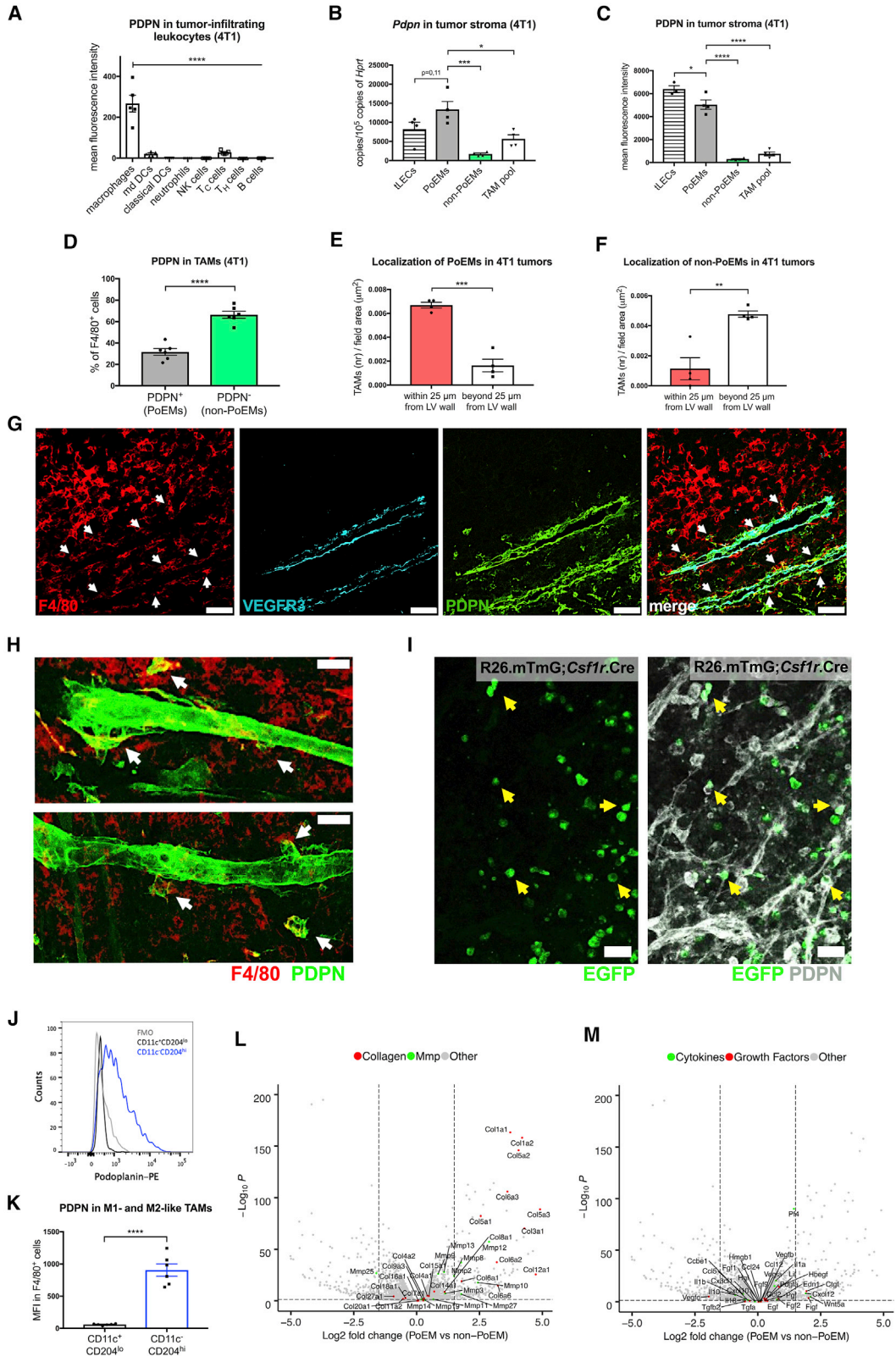

Figure 1. Podoplanin-Expressing Macrophages (PoEMs) Represent a Perilymphatic TAM Subset

(A–D) FACS analysis of the expression of PDPN in 4T1 tumor-infiltrating CD45$^+$ immune cells: macrophages (CD11b$^+$ and F4/80$^+$), monocyte-derived dendritic cells (DCs) (CD11b$^+$, CD11c$^+$, and F4/80$^-$), classical DCs (CD11b$^-$ and CD11c$^+$), neutrophils (CD11b$^+$and Ly6G$^+$), NK cells (NKp46$^+$), cytotoxic T cells

(legend continued on next page)

occurrence of lymphangiogenesis correlate with disease outcome in various tumor types, including breast cancer. Several soluble factors produced by lymphatic endothelial cells (LECs), cancer cells, or neighboring stromal cells have been implicated in the regulation of lymphangiogenesis and lymphoinvasion (including VEGFA, VEGFC, VEGFD, PDGFBB, and angiopoietins) (Stacker et al., 2014; Zheng et al., 2014).

Tumor-associated macrophages (TAMs) have critical roles at each stage of cancer progression (Mantovani, 2010; Nielsen and Schmid, 2017). However, the crosstalk between TAMs and lymphangiogenesis has not been extensively explored. One of the most relevant observations in the field is that TAM depletion in several tumor types abates VEGFC production and VEGFR3 signaling in LECs, thus impairing lymphangiogenesis (Ji et al., 2014). Nevertheless, molecular regulators of the interaction between TAMs and LECs are poorly characterized, and specific TAM subsets facilitating cancer cell intravasation into the LVs remain unidentified.

Podoplanin (PDPN) is a heavily O-glycosylated small mucin-type transmembrane glycoprotein with a wide variety of functions, including regulation of cell motility and adhesion (Astarita et al., 2012). Physiologically, CLEC2/PDPN interaction facilitates blood and LV separation during embryogenesis (Uhrin et al., 2010). In adult mice, PDPN in LECs prevents retrograde blood filling into the lymphatic system but does not affect LV patterning and function in healthy organs. The upregulation of PDPN correlates with malignant progression in several tumor types (Ugorski et al., 2016), including lymphatic metastasis in breast cancer (Braun et al., 2008). Despite being strongly expressed by LECs, PDPN is widely present in both cancer and tumor-infiltrating cells, e.g., in TAMs.

The roles of cancer-cell-derived PDPN in tumor progression have been well documented (Cueni et al., 2010; Suzuki et al., 2010). Conversely, the function of PDPN-expressing macrophages (PoEMs) and the importance of this molecule in TAMs have never been explored. Given the fact that TAMs expressing certain blood endothelial cell (BEC) markers, such as TIE2 (De Palma and Naldini, 2011), VEGFR1 (Shibuya, 2006), and NRP1 (Casazza et al., 2013), have already been implicated in angiogenesis, we wondered whether PDPN in macrophages plays a role in the growth of tumor lymphatics.

RESULTS

PoEMs Represent a Perilymphatic TAM Subset

Among all the cells of the immune system, we found that in orthotopic 4T1 breast tumors PDPN was almost exclusively expressed in TAMs, but not in other tumor-infiltrating leukocytes, as assessed by fluorescence-activated cell sorting (FACS) (Figure 1A). We also measured the transcript and protein levels of PDPN in different cell types, using freshly sorted tumor LECs (tLECs) as a reference. Strikingly, PoEMs had as much PDPN as tLECs (Figures 1B and 1C) (all qPCR primers used in this study are listed in Table S1). F4/80$^+$ skin macrophages or circulating monocytes from these tumor-bearing mice were, respectively, scarcely positive or negative for PDPN (Figures S1A and S1B). In line, PoEMs were nearly absent in resected LNs from both healthy and tumor-bearing mice (Figures S1C and S1D). These data suggest that PDPN expression becomes evident when monocytes differentiate into macrophages and experience some typical features of the tumor microenvironment such as hypoxia and/or TGFβ, which are known to promote *Pdpn* transcription (Suzuki et al., 2008; Tejchman et al., 2017).

Following these findings, we characterized TAM heterogeneity and distribution within the tumoral space. PDPN$^+$ TAMs (PoEMs) constituted about 30% of the entire TAM population infiltrating 4T1 breast tumors as shown by FACS (Figure 1D). Under histological assessment, we found that PoEMs were more proximal to the lymphatics than PDPN-negative TAMs (non-PoEMs) (Figures 1E–1G). Confocal imaging on thick sections from 4T1 breast tumors further confirmed that PoEMs localized in the proximity or adhered to the LV walls (Figure 1H). Next, we utilized the Rosa26.mTmG reporter line crossed with an inducible, macrophage-specific *Csf1r*.iCre deleter, which allowed us to distinguish TAMs (EGFP$^+$) from all the other stromal components (Tomato$^+$). In the syngeneic E0771 orthotopic breast cancer

(TCRβ$^+$, CD4$^-$, and CD8$^+$), T helper cells (TCRβ$^+$, CD4$^+$, and CD8$^-$), and B cells (CD19$^+$) (A). qRT-PCR analysis of the expression of *Pdpn* mRNA in stromal populations sorted from 4T1 tumors: LECs (CD45$^-$, CD31$^+$, and PDPN$^+$), PoEMs (CD45$^+$, CD11b$^+$, F4/80$^+$, and PDPN$^+$), non-PoEMs (CD45$^+$, CD11b$^+$, F4/80$^+$, and PDPN$^-$), and the total TAM pool (CD45$^+$, CD11b$^+$, and F4/80$^+$) (B). FACS analysis of the expression of PDPN in stromal populations in 4T1 tumors: LECs (CD45$^-$, CD31$^+$, and PDPN$^+$), PoEMs (CD45$^+$, CD11b$^+$, F4/80$^+$, and PDPN$^+$), non-PoEMs (CD45$^+$, CD11b$^+$, F4/80$^+$, and PDPN$^-$), and the total TAM pool (CD45$^+$, CD11b$^+$, and F4/80$^+$) (C). FACS analysis of PDPN$^+$ (PoEMs) and PDPN$^-$ (non-PoEMs) fractions in 4T1 TAMs (CD11b$^+$ and F4/80$^+$) (D).

(E and F) Immunofluorescent analysis of the localization of F4/80$^+$ and PDPN$^+$ (E) or F4/80$^+$and PDPN$^-$ (F) TAMs next to PDPN$^+$ and VEGFR3$^+$ LVs (within a distance of 25 μm from lymphatic vessel wall) and far from PDPN$^+$ and VEGFR3$^+$ LVs in 4T1 tumors. The number of cells was normalized per counting area (μm^2).

(G) Representative images of the localization of F4/80$^+$ and PDPN$^+$ (white arrows) or F4/80$^+$ and PDPN$^-$ TAMs in the proximity of and far from PDPN$^+$ and VEGFR3$^+$ LVs in 4T1 tumors.

(H) Representative confocal images of 100-μm 4T1 tumor sections demonstrating F4/80$^+$ and PDPN$^+$ TAMs (white arrows) in close proximity to PDPN$^+$ LVs.

(I) Representative confocal images of thick E0771 tumor sections implanted in ROSA$^{mT/mG}$;*Csf1r*.iCre mice, demonstrating EGFP$^+$ and PDPN$^+$ macrophages (yellow arrows) in the proximity of but not incorporated into PDPN$^+$ LVs.

(J and K) FACS analysis of the expression of PDPN in 4T1-derived TAM (CD11b$^+$ and F480$^+$) populations, namely M1 like (CD11c^{hi} and CD204^{lo}) and M2 like (CD11c^{lo} and CD204^{hi}). Similar results were obtained when gating for MHC II and CD206 for M1-like and M2-like populations (see also Figures S1E–S1G).

(L and M) Volcano plots showing the transcript distribution for several collagen subunits and MMPs (L) or cytokines and growth factors (M). The logarithms of the fold changes of individual genes (x axis) are plotted against the negative logarithm of their p value to base 10 (y axis). Positive $\log_2$ (fold change) values represent upregulation in PoEMs (sorted as triple-positive cells for CD11b, F4/80, and PDPN) compared to non-PoEMs (CD11b$^+$, F4/80$^+$, and PDPN$^-$ cells) out of the same tumor sample. Negative values represent downregulation. Dots above the horizontal dashed line represent differentially expressed genes with $p < 0.05$ after correction for multiple testing.

Statistical analysis: *$p < 0.05$; **$p < 0.005$; ***$p < 0.0005$; ****$p < 0.00005$. Graphs show mean ± SEM. Scale bars, 50 μm (G–I).

mT/mG, membrane-Tomato/membrane-GFP; DC, dendritic cells; PoEMs, podoplanin-expressing macrophages; non-PoEMs, podoplanin-negative macrophages; TAMs, tumor-associated macrophages; tLECs, tumor lymphatic endothelial cells.

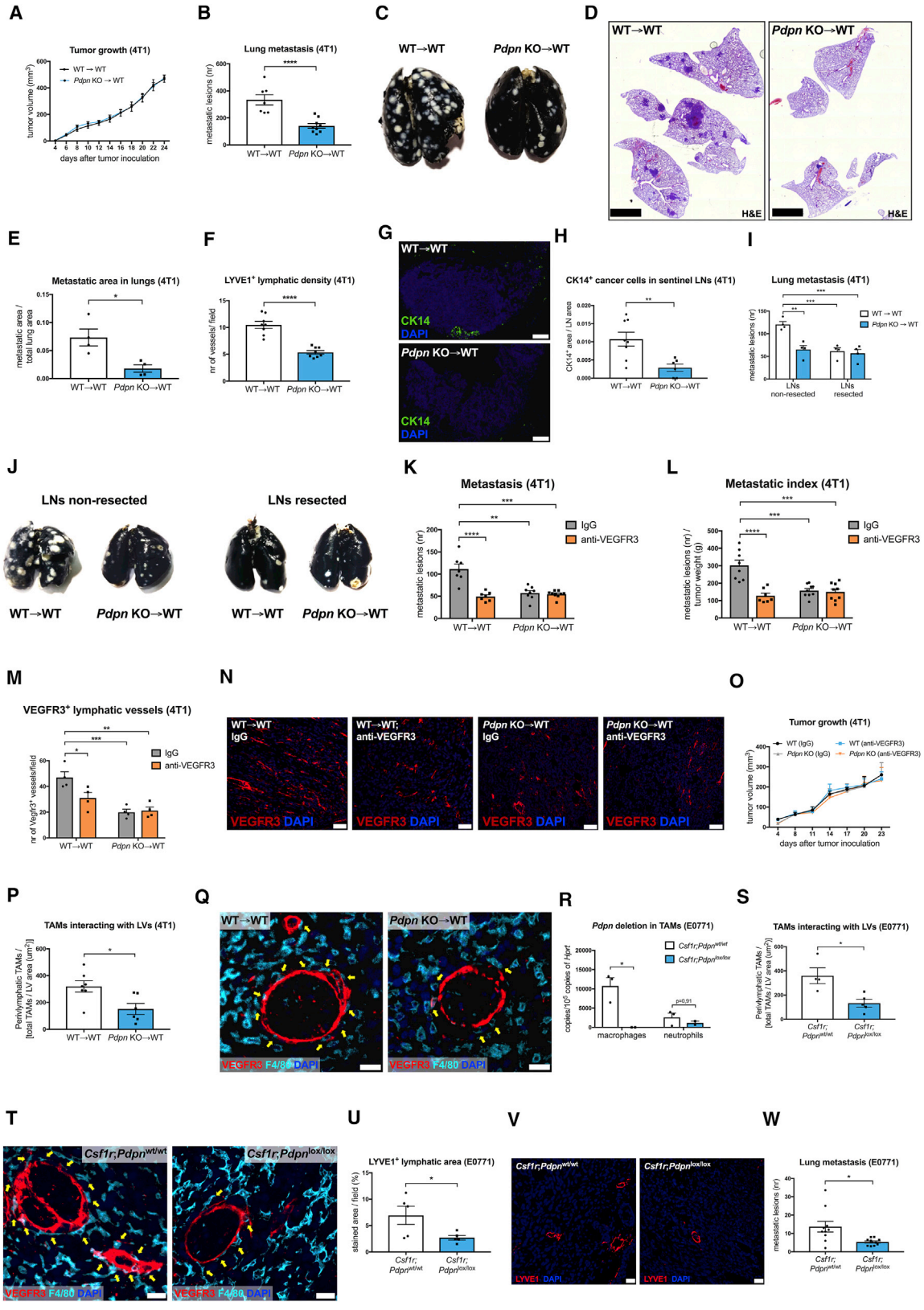

(legend on next page)

model, we observed that round-shaped, PDPN$^+$, and EGFP$^+$ TAMs were found adjacent to the LV walls (Figure 1I).

When characterizing the PoEM phenotype, we observed that MHC II^{lo}/CD206^{hi} or CD11c$^-$/CD204^{hi} F4/80$^+$ cells (pro-tumoral and M2 like) were highly positive for PDPN, while MHC II^{hi}/CD206^{lo} or CD11c$^+$/CD204^{lo} TAMs (anti-tumoral and M1 like) were PDPN low or negative (Figures 1J, 1K, and S1E–S1G) (Pucci et al., 2009). Besides, RNA sequencing (RNA-seq) analysis of PoEMs versus non-PoEMs revealed further transcriptomic differences (GEO: GSE126722). Gene ontology (GO) enrichment analysis pointed at a highly significant upregulation ($q < 0.005$) of processes related to extracellular matrix (ECM) remodeling and reorganization in PoEMs. In contrast, GO terms related to growth factor and cytokine signaling did not show any significant changes ($q > 0.005$) (Figure S1H; data not shown). Many matrix metalloproteinases (MMPs) and collagens, the main regulators of matrix organization and cancer invasion (Barcus et al., 2017; Clark and Vignjevic, 2015), were found strongly upregulated in PoEMs versus non-PoEMs (Figure 1L), while the majority of (lymph)angiogenic growth factors and cytokines did not show differential expression (Figure 1M). Overall, *Vegfc* and *Vegfd* (annotated as *Figf*), the two ligands of lymphangiogenic VEGFR3, were poorly expressed compared to *Vegfa* (Figure S1I). Together, these data suggest that PoEMs represent a subset of TAMs potentially involved in matrix turnover and invasion.

Pdpn Deletion in TAMs Inhibits Tumor Lymphatic Growth and Metastasis and Impairs Perilymphatic Localization of TAMs

To study the biological function of PDPN in TAMs, wild-type (WT), and *Pdpn* knockout (KO), bone marrow (BM) cells were used to reconstitute the immune system of lethally irradiated WT Balb/c recipient mice, thus generating WT→WT and *Pdpn* KO→WT chimeras (Figure S2A). Six weeks after BM reconstitution, syngeneic 4T1 breast cancer cells were injected orthotopically in both WT→WT and *Pdpn* KO→WT mice. Despite comparable tumor growth, pulmonary metastases were 60% lower in KO→WT versus WT→WT mice (Figures 2A–2E, S2B, and S2C). This was not caused by differential cancer cell extravasation and lodging to the lungs, as the number of pulmonary nodules following intravenous injection of 4T1 cancer cells was comparable in WT→WT and KO→WT mice (Figure S2D). Similar to human triple-negative breast cancer (TNBC), 4T1 cancer cells disseminate preferentially via the lymphatic route and to a lower extent via blood vessels (Mohammed et al., 2011; Pulaski and Ostrand-Rosenberg, 2001; Ran et al., 2010). We therefore focused our attention on tumor LVs and LN metastasis. Density, total area, and lumen size of lymphatics were strongly (up to 75%) reduced in KO→WT versus WT→WT mice, as assessed by the usage of various lymphatic endothelium markers, i.e., LYVE1, VEGFR3, and PROX1 (Figures 2F and S2E–S2K). This impaired lymphangiogenesis was associated with decreased Evans blue drainage from the tumor to the inguinal LNs (Figure S2L). Consistently, the number of CK14$^+$ breast cancer cells in the draining LNs was 75% lower in KO→WT versus WT→WT mice (Figures 2G and 2H). On the other hand, tumor blood vessel density and area, as well as pericyte coverage, permeability, and tumor hypoxia (parameters linked to cancer cell intravasation into the bloodstream) (Mazzone et al., 2009) were not affected by *Pdpn* deletion (Figures S2M–S2S).

In order to further compare the rates of hematogenous and lymphatic dissemination, we assessed lung metastasis in WT→WT and KO→WT mice wherein the draining LNs were resected (or not) prior to orthotopic 4T1 tumor implantation. LN resection in WT→WT mice reduced lung metastasis by 55%, but it did not result in any additional effect in the KO→WT mice, suggesting that tumor blood vessel intravasation and hematogenous metastasis stayed unaltered (Figures 2I and 2J). Consistent with our observation that PoEMs are absent in LNs, the blood or lymph vessel density in the draining LNs of WT→WT and KO→WT tumor-bearing mice were the same (Figures S2T–S2V). Moreover, the injection of 4T1 cells directly into the draining LNs resulted in comparable lung metastasis (Figure S2W).

Based on the finding that PDPN in TAMs is relevant for LV growth and lymphatic metastasis, we hypothesized that standard anti-lymphangiogenic therapy would be ineffective in *Pdpn* KO→WT tumor-bearing mice. In WT→WT mice, a

Figure 2. Deletion of PDPN in TAMs Inhibits Tumor Lymphatic Growth and Metastasis

(A–E) 4T1 tumor growth (A), lung metastasis (B), representative images of black-ink-injected lungs from 4T1 tumor-bearing mice (C), representative images of lung sections stained with H&E (D), and histologically assessed metastatic area in lungs (E) of WT→WT or *Pdpn* KO→WT chimeras. Data show representative values of 4 independent experiments.

(F) Quantifications of 4T1 tumor sections stained for a lymphatic endothelial cell-specific marker LYVE1.

(G and H) Representative images and quantifications of inguinal lymph nodes from 4T1 tumor-bearing mice, stained for cytokeratin 14 (CK14) as a marker of cancer cells.

(I and J) Quantification of lung metastasis (I) and representative images of black-ink-injected lungs (J) from mice in which lymphadenectomy of tumor-draining lymph nodes was performed 7 days prior to 4T1 cell inoculation.

(K–O) Quantification of lung metastasis (K), metastatic index (L), VEGFR3$^+$ lymphatics in tumors (M), representative images of tumor sections stained for VEGFR3 (N), and 4T1 tumor growth (O) in WT→WT and *Pdpn* KO→WT mice treated with a VEGFR3-blocking antibody (Mf431C1) or isotype (rat IgG) control by bi-weekly intratumoral injections (40 μg per 1 g of body weight).

(P and Q) Quantification (P) and representative images (Q) of F4/80$^+$ TAMs (yellow arrows) directly interacting with VEGFR3$^+$ LVs in 4T1 tumors.

(R) qRT-PCR for *Pdpn* mRNA in CD11b$^+$, F4/80$^+$ TAMs and CD11b$^+$, Ly6G$^+$ neutrophils isolated from E0771 tumors grown in *Csf1r*;*Pdpn*$^{wt/wt}$ or *Csf1r*;*Pdpn*$^{lox/lox}$ mice.

(S and T) Quantification (S) and representative images (T) of F4/80$^+$ TAMs (yellow arrows) directly interacting with VEGFR3$^+$ LVs in E0771 tumors.

(U and V) Quantification (U) and representative images (V) of E0771 tumor sections stained for a lymphatic endothelial cell marker LYVE1.

(W) E0771 lung metastasis.

Statistical analysis: *$p < 0.05$; **$p < 0.005$; ***$p < 0.0005$; ****$p < 0.00005$. Graphs show mean ± SEM. Scale bars, 20 μm (N, Q, and T), 50 μm (V), 100 μm (G), and 2.5 mm (D).

DAPI, 49,6-diamidino-2-phenylindole.

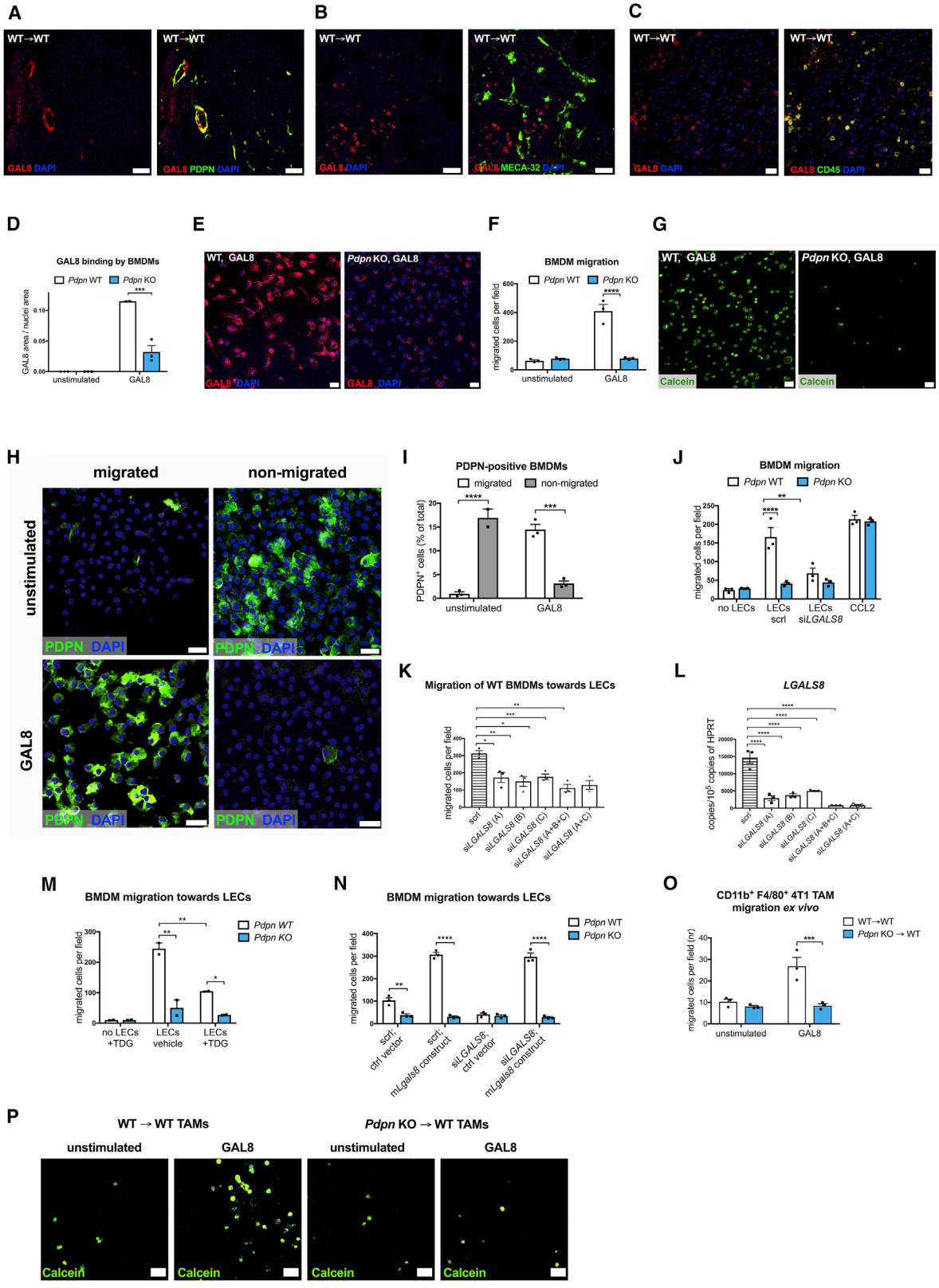

Figure 3. Perilymphatic Macrophage Localization Is Mediated by GAL8 Expression in LECs

(A–C) Representative images of 4T1 tumor sections stained for GAL8 and PDPN (A), GAL8 and MECA-32 (B), and GAL8 and CD45 (C).

(D and E) Quantification (D) and representative images (E) of WT or *Pdpn* KO BMDMs stained for GAL8 upon 40 min incubation with recombinant murine GAL8 (0.5 μM) or PBS (unstimulated).

(legend continued on next page)

VEGFR3-blocking antibody (clone mF431C1) (Laakkonen et al., 2007) reduced 4T1 tumor lymph vessel formation and metastasis by 50% and 40%, respectively (Figures 2K–2N). However, anti-VEGFR3 had no effect on tumor lymphangiogenesis and dissemination in KO→WT chimeras. Tumor growth was comparable in all the groups (Figure 2O). Altogether, these data indicate that PoEMs promote tumor lymphangiogenesis and lymphatic metastasis, likely favoring cancer cell entry into the lymphatic circulation.

As TAMs were the main population of leukocytes expressing PDPN (Figure 1A), we analyzed CD11b$^+$, F4/80$^+$ macrophages from 4T1 tumors (Figure S3A) and confirmed *Pdpn* deletion in KO→WT mice by both FACS and qRT-PCR (Figures S3B and S3C). *Pdpn* knockout did not influence overall TAM infiltration (Figures S3D and S3E). However, the interaction of TAMs with LVs was strongly impaired in the absence of PDPN (Figures 2P, 2Q, and S3F). In contrast, TAM contact with tumor blood vessels did not change significantly in *Pdpn* WT versus KO→WT mice (Figures S3G and S3H). Although PDPN was relevant for TAM attachment to the lymphatics, its deletion did not affect the expression of main M1 or M2 macrophage polarization markers, defining pro-inflammatory or pro-(lymph)angiogenic macrophage subsets, respectively (Figures S3I–S3L). Similarly, whole tumors and TAMs from *Pdpn* WT and KO chimeras had comparable levels of *Vegfa*, *Vegfc*, and *Vegfd* (Figures S3M–S3P). In line with the RNA-seq data, while TAMs have high levels of *Vegfa*, they represent a poor source of *Vegfc* as compared to the rest of the tumor, including cancer cells and cancer-associated fibroblasts (CAFs) (Figure S3Q).

In a different orthotopic breast cancer model—EMT6.5, KO→WT mice also had impaired perilymphatic TAM distribution, diminished LV area, and reduced metastatic burden, despite unaltered tumor growth (Figures S4A–S4H). Moreover, in mice lacking *Pdpn* specifically in TAMs upon Tamoxifen treatment (Figure 2R), orthotopic E0771 breast tumors displayed defective perilymphatic TAM localization (Figures 2S, 2T, and S4I) as well as diminished lymphangiogenesis and metastasis, while tumor growth was comparable in all the groups (Figures 2U–2W and S4J–S4O). Blood vessel density, pericyte coverage, tumor hypoxia, and TAM infiltration were not altered by macrophage-specific *Pdpn* deletion (Figures S4P–S4U).

Finally, existing LVs in adult skin (Figures S5A and S5B) as well as pathological (lymph)angiogenesis in cauterized corneas (Figures S5C–S5F), were both comparable in WT→WT and KO→WT chimeras, consistent with the absence of PoEMs in these conditions (data not shown). Overall, we found that PDPN expression is (1) the highest in pro-tumoral M2-like TAMs, (2) crucial for PoEM localization around the lymphatics, but (3) dispensable for determining their differentiation state into canonical M1 versus M2 macrophages. The impairment of the recruitment of a PDPN$^+$ TAM subset to the perilymphatic space results in reduced tumor lymphangiogenesis in KO→WT mice, with a consequent decrease in lymphatic metastasis.

Perilymphatic TAM Localization Is Mediated by GAL8 Expression in LECs

Given the perilymphatic localization defect of macrophages, we focused our attention on a known PDPN interactor—galectin 8 (GAL8)—a secreted glycan-binding protein abundantly expressed by LVs, modulating cell adhesion and migration, codified by the gene *LGALS8* (Troncoso et al., 2014). First, we analyzed GAL8 expression in 4T1 tumor sections and found that this protein is expressed by tumor lymphatics and some CD45$^+$ infiltrating immune cells but not by tumor blood vessels (Figures 3A–3C). *In vitro*, LECs defined as CD31$^+$, PDPN$^+$ cells (Figure S6A) expressed *LGALS8* but did not express the most studied PDPN ligand—*CLEC2* (Figure S6B). In line with the *in vivo* distribution, *LGALS8* expression in cultured LECs was 3.2 times higher than in BECs (Figure S6C) and not detected in 4T1 or E0771 breast cancer cells (Figure S6D).

Next, we validated GAL8 binding to *Pdpn* WT BM-derived macrophages (BMDMs), also expressing PDPN at the mRNA and protein levels (Figures S6E and S6F). GAL8 binding was impaired by 70% in *Pdpn* KO BMDMs (Figures 3D and 3E). When measuring the migratory capacity of macrophages in a transwell assay, WT BMDMs migrated efficiently toward recombinant GAL8, whereas *Pdpn* KO BMDMs showed an almost complete lack of migratory response (Figures 3F and 3G). Interestingly, in the WT condition, BMDMs that migrated toward GAL8 were PDPN positive, whereas the non-migrated ones did not express PDPN, as assessed by immunofluorescent staining (Figures 3H and 3I). This finding suggested that only PDPN-positive macrophages were attracted by GAL8 and was consistent with the observation that macrophages differentiated *in vitro* from BM cells constitute a mixed population, in which about

(F and G) Quantification (F) and representative images (G) of WT or *Pdpn* KO calcein-labeled BMDM migration through 8 μm pores (transwell) in response to recombinant murine GAL8 (0.5 μM) or control medium (unstimulated).

(H and I) Representative images (H) and quantification (I) of WT BMDM migration through 8 μm pores (transwell) in response to murine recombinant GAL8 (0.5 μM) or normal medium (unstimulated). Migrated and non-migrated BMDM fractions were stained for PDPN and DAPI.

(J) Quantification of WT or *Pdpn* KO BMDM migration through 8 μm pores (transwell) in response to soluble factors released by LECs (HMVECs and human microvascular endothelial cells) silenced (si*Lgals8*) or not silenced (scrl) for *Lgals8*, a gene encoding GAL8. CCL2 was used as a positive control.

(K and L) Quantification of the migration of WT BMDMs through 8 μm pores in response to LEC-derived soluble factors (K). LECs were silenced for *Lgals8* using 3 different siRNA probes separately or in combination (L). scrl, scrambled control.

(M) Quantification of WT or *Pdpn* KO BMDMs migration through 8 μm pores in response to LEC-derived soluble factors. LECs were cultured with a GAL8 inhibitor (TDG, 20 mM). Data show representative values of two independent experiments.

(N) Quantification of WT or *Pdpn* KO BMDM migration through 8 μm pores (transwell) in response to soluble factors released by HMVECs, silenced (si*LGALS8*) or not silenced (scrl) for *LGALS8*, a gene encoding GAL8. Prior to the migration assay, LECs were transduced with a viral vector carrying a plasmid overexpressing murine *Lgals8* or a control plasmid (see also Figures S6G and S6H).

(O and P) Quantification (O) and representative images (P) of the migration of calcein-labeled CD11b$^+$, F4/80$^+$ TAMs sorted from 4T1 tumors bore by WT→WT and *Pdpn* KO→WT chimeras. The migration through 8 μm pores occurred in response to recombinant murine GAL8. The graph shows values of three biological repetitions per condition.

Statistical analysis: *$p < 0.05$; **$p < 0.005$; ***$p < 0.0005$; ****$p < 0.00005$. Graphs show mean ± SEM. Scale bars, 20 μm (B, C, E, G, and H) and 50 μm (A and P). CCL2, chemokine (C-C motif) ligand 2; DAPI, 49,6-diamidino-2-phenylindole; scrl, scrambled control; LEC, lymphatic endothelial cells; TDG, thiodigalactoside.

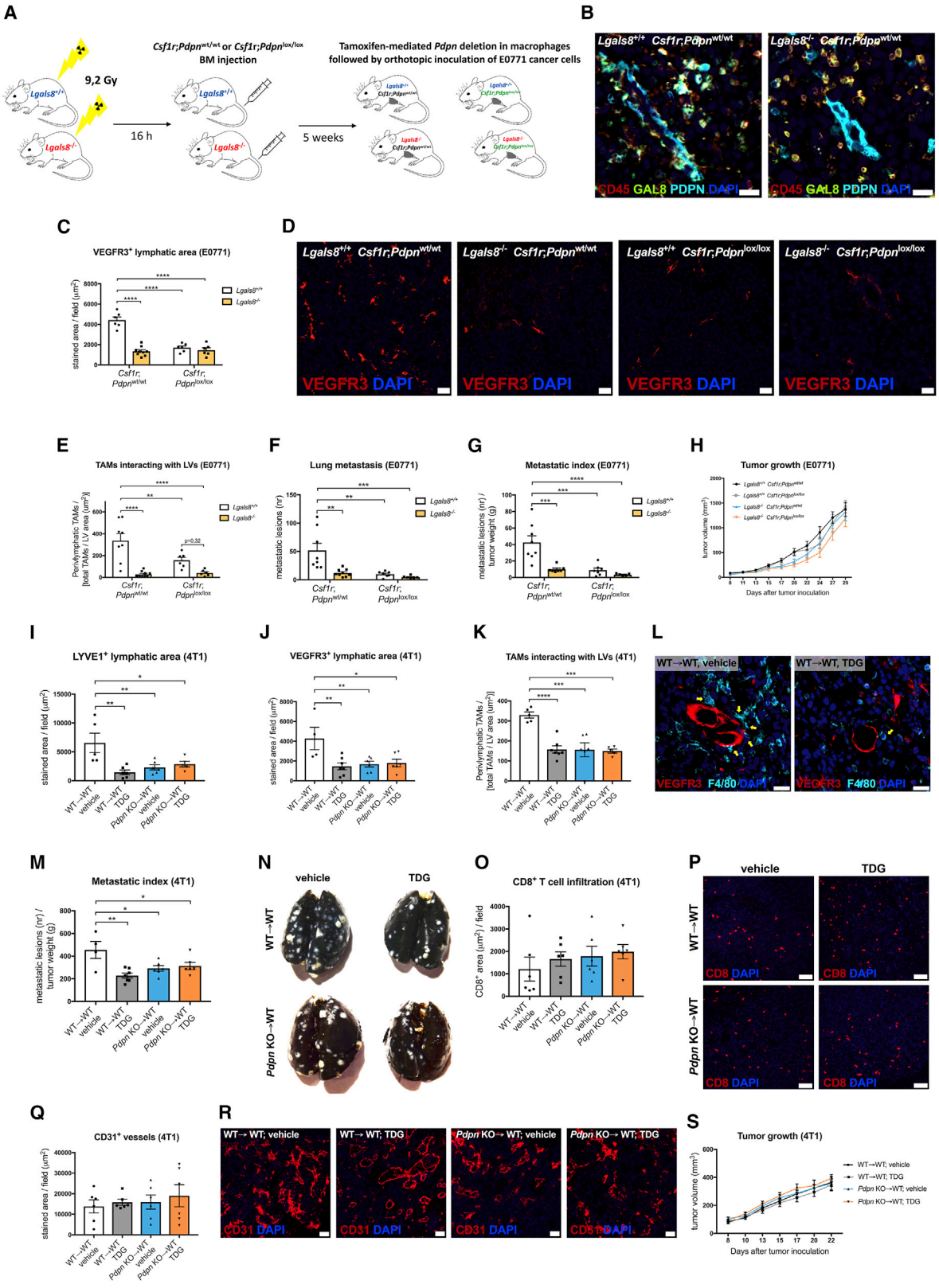

(legend on next page)

20% of cells are PDPN positive and the remaining 80% are PDPN negative (Figure S6E). Furthermore, WT, but not KO, BMDMs were able to migrate toward a monolayer of LECs (Figure 3J). Silencing of *LGALS8* in LECs with three different siRNAs (or combinations of those) (Figures 3J–3L) or pharmacologic inhibition of GAL8 with thiodigalactoside (TDG) (Figure 3M) impaired the migration of WT BMDMs to the same extent as the knockout of *Pdpn*, but it did not further affect the migratory behavior of *Pdpn* KO macrophages. As a positive control, we show that the migratory capacity toward CCL2 was comparable for both WT and *Pdpn* KO BMDMs (Figure 3J). *Lgals8* reconstitution in *LGALS8*-silenced LECs restored macrophage chemoattraction, excluding possible off-target effects (Figures 3N, S6G, and S6H). In line with these results, *Pdpn* deficiency strongly impaired the *ex vivo* migration of sorted TAMs toward GAL8 (Figures 3O and 3P). Therefore, our data demonstrate that GAL8 expression by the LVs is important for macrophage migration toward LECs.

In order to validate the significance of LV-derived GAL8 for TAM recruitment into the perilymphatic space, we generated a pseudo-specific knockout of GAL8 in tumor lymphatics. To this end, *Lgals8* WT and KO recipient mice were reconstituted with BM cells from *Csf1r*.iCre × *Pdpn*$^{lox/lox}$ mice (or from *Csf1r*.iCre × *Pdpn*$^{wt/wt}$ controls) (Figure 4A). Since in tumors GAL8 was expressed by leukocytes and lymphatics only (Figures 3A–3C), this procedure restricted *Lgals8* deficiency to LVs, whereas CD45$^+$ immune cells still expressed GAL8 (Figure 4B). Genetic deletion of *Lgals8* in LECs strongly decreased tumor LV area and the attachment of *Pdpn* WT TAMs to tumor lymphatics (Figures 4C–4E). This was accompanied by a reduction in lung metastasis (Figures 4F and 4G). Conversely, *Lgals8* deletion in the context of *Pdpn* KO TAMs did not further affect tumor LVs, perilymphatic TAM distribution, or the metastatic burden observed in *Pdpn* KO chimeras. All experimental groups showed comparable tumor growth (Figure 4H).

Next, we utilized TDG in order to provide a proof of concept of pharmacologic GAL8 targeting, even though TDG is not a specific GAL8 inhibitor as its mode of action also restrains Galectin 1, Galectin 3, and Galectin 9 (Tribulatti et al., 2012). TDG is a non-metabolized synthetic disaccharide that works as a glycomimetic agent. Its sugar segment targets the binding pocket in galectins' carbohydrate recognition domains (Laaf et al., 2019). For this approach, we chose another breast cancer model—4T1 (instead of E0771 tumors as in the above-mentioned genetic targeting). Intratumoral injection of TDG (Ito et al., 2011) in WT→WT mice led to similar effects as those observed in the *Lgals8* KO recipients, namely decreased lymphangiogenesis, less TAM-LV interactions, and reduced lung metastasis (Figures 4I–4N). In *Pdpn* KO→WT mice, TDG treatment did not additionally influence the lymphatic phenotype. Although galectins can affect blood vessel formation and CD8$^+$ T cell activation (Ito et al., 2011; Markowska et al., 2010), tumor growth, tumor blood vessel density, and CD8$^+$ T cell infiltration were not influenced by TDG treatment in our model (Figures 4O–4S). Altogether, these data argue that GAL8 in breast tumor lymphatics and PDPN in TAMs participate in the same molecular process and emerge as key factors of a previously unexplored metastatic cascade in breast cancer.

PoEM Migration and Adhesion Depend on GAL8-Mediated Integrin β1 Activation

GAL8 binding to PDPN was reported to favor clustering and activation of integrin β1 (CD29) in LECs (Chen et al., 2016). Given the adhesion defects observed in *Pdpn* KO BMDMs, we wondered whether similar effects occur on the PoEM (macrophage) surface. Indeed, we found that GAL8 stimulation induced integrin β1 activation in *Pdpn* WT, but not in KO, BMDMs (Figures 5A and 5B) and that GAL8 binding to *Itgb1*-silenced BMDMs was decreased to the same level as in *Pdpn* KO BMDMs (Figures S6I–S6K). No additional impairment of GAL8 binding was observed upon silencing of integrin β1 in *Pdpn* KO BMDMs. Next, we found that PDPN and β1 integrin interaction was promoted by GAL8 stimulation in *Pdpn* WT, but not in *Pdpn* KO, BMDMs, as assessed by a proximity ligation assay (PLA) (Figures 5C and 5D) and co-immunoprecipitation for PDPN and the integrin β1 subunit (Figure S6L). In line with the fact that

Figure 4. Genetic Deletion of *Lgals8* in Lymphatics or Pharmacologic Inhibition of GAL8 Prevents Lymphatic Growth and PoEM-Dependent Lymphoinvasion

(A) Scheme illustrating generation of *Csf1r*;*Pdpn*$^{wt/wt}$ or *Csf1r*;*Pdpn*$^{lox/lox}$ chimeras upon lethal irradiation of Lgals8$^{+/+}$ or Lgals8$^{-/-}$ mice and subsequent BM reconstitution. Five weeks after the procedure, mice were injected intraperitoneally for 5 consecutive days with 1 mg of tamoxifen in order to ensure *Pdpn* deletion in *Csf1r*$^+$ cells (macrophages) of the *Csf1r*;*Pdpn*$^{lox/lox}$ group. Next, the chimeras were orthotopically injected with E0771 breast cancer cells. Gy, gray.

(B) Representative images of E0771 tumor sections stained for CD45, GAL8, and PDPN, demonstrating that the deletion of GAL8 in Lgals8$^{-/-}$, *Csf1r*;*Pdpn*$^{wt/wt}$ chimeras is restricted to PDPN$^+$ LVs.

(C and D) Quantifications and representative images of E0771 tumor sections stained for a lymphatic endothelial cell marker VEGFR3.

(E) Quantification of F4/80$^+$ TAMs directly interacting with VEGFR3$^+$ LVs in E0771 tumors, assessed by immunostaining.

(F–H) Lung metastasis (F), metastatic index (G), and E0771 tumor growth (H) of *Csf1r*;*Pdpn*$^{wt/wt}$ or *Csf1r*;*Pdpn*$^{lox/lox}$ BM chimeras generated in Lgals8$^{+/+}$ or Lgals8$^{-/-}$ mice.

(I and J) Quantifications of 4T1 tumor sections stained for lymphatic endothelial cell markers, i.e., LYVE1 (I) and VEGFR3 (J). The tumors were injected with a GAL8 inhibitor (TDG, 120 mg/kg body weight) or vehicle (PBS) three times per week throughout the experiment.

(K and L) Quantification (K) and representative images (L) of F4/80$^+$ TAMs (yellow arrows) directly interacting with VEGFR3$^+$ LVs in 4T1 tumors injected tri-weekly with TDG (120 mg/kg) or vehicle (PBS).

(M and N) Metastatic index (M) and representative images of black-ink-injected lungs from 4T1 tumor-bearing mice (N). Tumors were injected tri-weekly with TDG (120 mg/kg) or vehicle (PBS).

(O and P) Quantification (O) and representative images (P) of CD8$^+$ T cells infiltrating 4T1 tumors injected tri-weekly with TDG (120 mg/kg) or vehicle (PBS).

(Q and R) Quantification (Q) and representative images (R) of CD31$^+$ blood vessels in 4T1 tumors injected tri-weekly with TDG (120 mg/kg) or vehicle (PBS).

(S) 4T1 tumor growth in WT→WT and *Pdpn* KO→WT mice. The tumors were injected tri-weekly with TDG (120 mg/kg) or vehicle (PBS).

Statistical analysis: *$p < 0.05$; **$p < 0.005$; ***$p < 0.0005$; ****$p < 0.00005$. Graphs show mean ± SEM. Scale bars, 20 μm (B, D, L, and R) and 50 μm (P).

DAPI, 49,6-diamidino-2-phenylindole; TDG, thiodigalactoside.

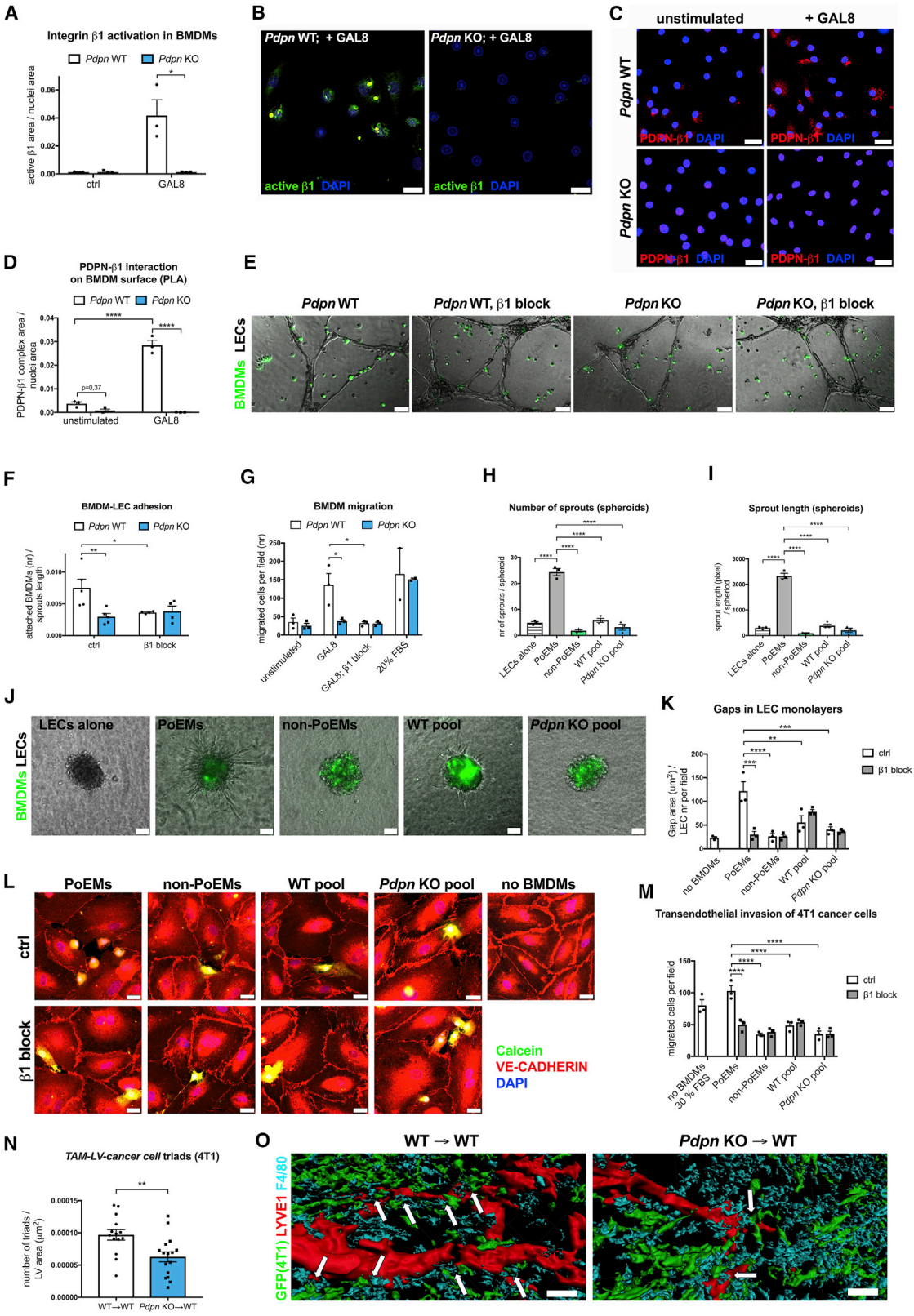

Figure 5. PDPN-Mediated Adhesion of PoEMs to LECs Promotes Lymphatic Growth and Cancer Cell Lymphoinvasion

(A and B) Quantification (A) and representative images (B) of WT or *Pdpn* KO BMDMs stained for activated form of integrin β1 (9EG7) upon 40 min treatment with recombinant murine GAL8 (0.5 μM) or normal medium (ctrl).

(legend continued on next page)

integrin β1 signaling is crucial for macrophage migration (Meng and Lowell, 1998), the deactivation of β1 on WT BMDMs (with a blocking antibody or with siRNAs) impaired their *in vitro* adhesion to LECs (Figures 5E and 5F) or their migration toward GAL8 (Figure 5G). This effect was specifically dependent on integrin β1, but not on integrin β2 (Figures S6M–S6O). Altogether, these data support the idea that the binding of GAL8 to PDPN on the macrophage surface promotes the formation of a multicomplex with β1 integrin and ultimately its activation—a pre-requisite for macrophage migration and adhesion to LECs.

PDPN-Mediated Adhesion of PoEMs to LECs Promotes Lymphatic Growth and Cancer Cell Lymphoinvasion

To assess the functional relevance of our findings, we conducted a capillary network formation assay where *Pdpn* WT or KO BMDMs were seeded together with LECs. In these conditions, LECs cultured with *Pdpn* KO BMDMs formed simpler, less dense lymphatic networks in comparison to those observed in the presence of WT BMDMs (Figures S6P and S6Q). Then, using a 3D spheroid sprouting assay in a type I collagen gel, we demonstrated that BMDMs increased the number and length of sprouts formed by LECs. Moreover, this lymphangiogenic effect was much stronger when the same assay was performed by adding PoEMs to the spheroid (instead of a total WT BMDM pool) (Figures 5H–5J). Neither *Pdpn* KO nor WT PDPN-negative BMDMs elicited any sprouting effect. In contrast, PoEMs, non-PoEMs, total *Pdpn* WT, and KO BMDMs triggered a similar proliferative boost when co-cultured with LECs (Figure S6R); LEC apoptosis was scarce and not increased in any of the conditions tested (Figure S6S). Altogether, these data indicate that PDPN in PoEMs is important for sustaining LV sprouting but not for LEC proliferation and survival.

Macrophage proximity to blood vessels has been shown to modulate endothelial junctions and favor blood vessel intravasation of cancer cells through their direct interaction, resulting in the formation of TAM-cancer cell-BEC triads (Harney et al., 2015). We therefore set up a system where we evaluated how different sorted populations of F4/80$^+$ BMDMs were remodeling VE-cadherin junctions of a confluent LEC monolayer. We found that the opening of the endothelial layer was much stronger in the presence of PDPN$^+$ macrophages, but not with PDPN$^-$ or *Pdpn* KO macrophages (Figures 5K and 5L). Aligned with these results, transendothelial migration of calcein-labeled 4T1 cancer cells was promoted by PDPN$^+$, but not by PDPN$^-$ or *Pdpn* KO macrophages (Figure 5M). Pre-incubation of macrophages with the integrin β1 blocker prevented PoEM-induced formation of interendothelial gaps and 4T1 cancer cell transmigration (Figures 5K–5M). Thus, PoEM adhesion to the lymphatic endothelium is sufficient to induce gaps in a LEC monolayer and facilitate cancer cell transmigration.

In light of the above findings, we assessed the presence of triads at the LV site by implanting GFP-expressing 4T1 tumors into BM chimeras. In WT→WT mice, clusters of LECs, macrophages, and GFP$^+$ cancer cells were frequently found, while their presence was reduced by 35 % in the KO→WT mice (even when normalized for strongly reduced LV area) (Figures 5N, 5O, S6T, and S6U). Together, these data suggest that PoEMs at the LVs are instrumental for the promotion of lymphatic growth and cancer cell lymphoinvasion.

PDPN in PoEMs Serves as an Upstream Regulator of Matrix Remodeling

Based on the initial RNA-seq-based observations (Figures 1L and S1H), we hypothesized that PDPN could be involved upstream in the transcriptional regulation of certain genes. We arbitrarily focused on the top 100 upregulated (and not downregulated) transcripts (false discovery rate (FDR) < 0.05), taking into account the mediators of matrix composition and digestion, i.e., collagens and MMPs, located at the right side of the volcano plot (Figure 1L). We identified a list of 4 MMPs (*Mmp2*, *Mmp9*, *Mmp12*, and *Mmp13*) and 8 collagen subunit genes (*Col1a1*, *Col1a2*, *Col3a1*, *Col5a2*, *Col5a3*, *Col5a1*, *Col6a2*, and *Col6a3*), which were highly upregulated in PoEMs versus non-PoEMs. Using independent cohorts of mice, we confirmed that PoEMs had the highest expression levels of all these genes, while non-PoEMs, *Pdpn* WT, and KO TAMs showed lower transcript values (Figures 6A–6M). *Vegfa*, *Vegfc*, and *Vegfd* were equally expressed in both PoEMs and non-PoEMs as well as in their total pool, and their expression did not change in *Pdpn* KO TAMs (Figures 6N–6P).

Lymphatic capillaries attach directly to the interstitial matrix, mainly composed of fibrillar type I collagen (Detry et al., 2011). Interestingly, PoEMs, constituting a TAM subset proximal to tumor lymphatics, abundantly express *Col1a1* and *Col1a2*

(C and D) Representative images (C) and quantification (D) of the proximity ligation assay (PLA) between PDPN and integrin β1 on the surface of WT or *Pdpn* KO BMDMs. BMDMs were treated for 40 min with recombinant murine GAL8 (0.5 μM) or normal medium (unstimulated) prior to the assay.

(E and F) Representative images (E) and quantification (F) of WT or *Pdpn* KO calcein-labeled BMDMs adhering to preformed lymphatic capillary-like structures (HMVECs). Prior to the assay, BMDMs were incubated for 20 min with an integrin β1-blocking antibody (HMβ1-1) or isotype control.

(G) Quantification of *Pdpn* WT or *Pdpn* KO BMDM migration through 8 μm pores (transwell) in response to murine recombinant GAL8 (0.5 μM). Prior to the migration, BMDMs were incubated for 20 min with an integrin β1-blocking antibody (HMβ1-1) or isotype control.

(H–J) Quantifications of the number of sprouts (H), total sprout length (I), and representative images (J) of LEC (HMVEC) spheroids embedded in collagen I with various sorted BMDM populations (or alone) for 24 h.

(K and L) Quantification (K) and representative images (L) of intercellular gaps between HMVECs cultured in monolayers for 5 days and incubated together with different populations of sorted, calcein-labeled BMDMs for 16 h. The co-cultures were fixed and stained for VE cadherin, enabling the visualization of cell-cell junctions.

(M) Quantification of calcein-labeled 4T1 cancer cell migration through LEC monolayers (seeded on 8 μm pore-transwells) incubated for 16 h with different populations of sorted BMDMs. Prior to the assay, BMDMs were incubated for 20 min with an integrin β1-blocking antibody (HMβ1-1) or isotype control.

(N and O) Quantification (N) and representative 3D reconstructions (O) of confocal images of 4T1-GFP$^+$ tumor sections stained for LYVE1, F4/80, and GFP. White arrows demonstrate the presence of TAMs-LVs-4T1 cancer cells triads. The numbers of triads were normalized per LYVE1$^+$ lymphatic vessel area. The average number of triads per tumor and total lymphatic vessel area are shown in Figures S6T and S6U.

Statistical analysis: *$p < 0.05$; **$p < 0.005$; ***$p < 0.0005$; ****$p < 0.00005$. Graphs show mean ± SEM. Scale bars, 20 μm (B, C, E, and L) and 40 μm (O).

DAPI, 49,6-diamidino-2-phenylindole; PoEMs, podoplanin-expressing macrophages; non-PoEMs, podoplanin-negative macrophages.

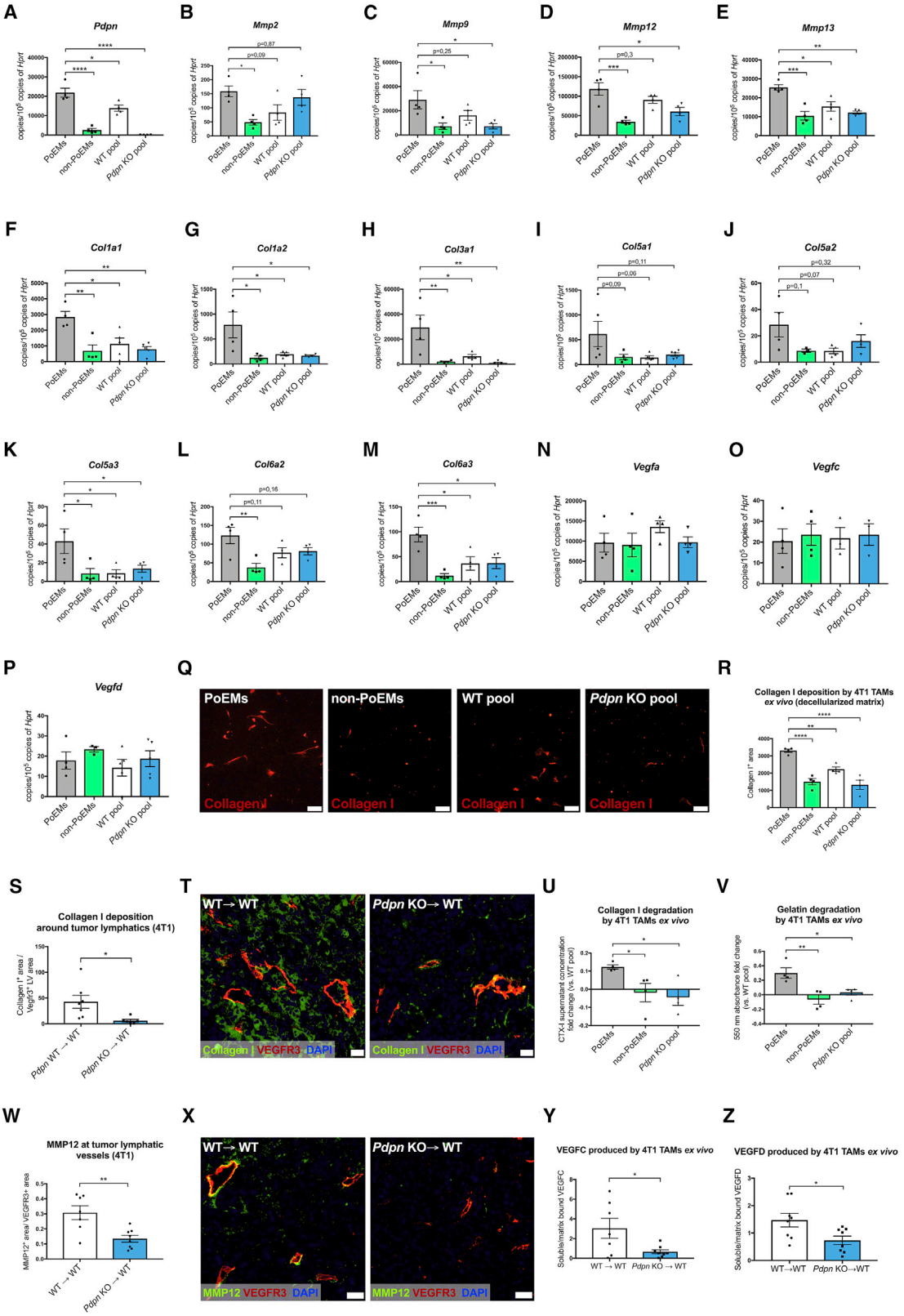

Figure 6. PDPN in PoEMs Is the Upstream Regulator of Matrix Remodeling, Independent of GAL8 Binding

(A–M) qRT-PCR analysis of the expression of *Mmps* and *collagen* subunits in CD11b^{+}, F4/80^{+} TAM populations sorted from 4T1 tumors: PoEMs (PDPN^{+}), non-PoEMs (PDPN^{-}), the total WT TAM pool, and the total *Pdpn* KO TAM pool (PDPN^{-}).

(legend continued on next page)

subunits. Consistently, bundles of type I collagen were richly deposited by *ex vivo* cultured PoEMs and less were deposited by non-PoEMs and *Pdpn* KO TAMs, while total *Pdpn* WT TAMs displayed an intermediate collagen I deposition state, as assessed by stainings on the decellularized matrix (Figures 6Q and 6R). In histology, 4T1 tumor sections had thinner sleeves of type I collagen around LVs in KO→WT versus WT→WT mice (Figures 6S and 6T).

CTX-Is are C-terminal telopeptides that are released during type I collagen digestion (Garnero et al., 2003). Consistent with the highest levels of *Mmp2*, *Mmp9*, *Mmp12*, and *Mmp13* (and other MMPs that were further down in the list of upregulated genes), PoEMs displayed the strongest collagen degradation activity (Figure 6U) and the highest gelatinase activity, the latter ascribed to MMP2, MMP9, and MMP12 (Chelluboina et al., 2015; Jacob et al., 2013; Li et al., 2012) (Figure 6V). Consistently, tumor LVs in the KO→WT mice had 60% less perilymphatic MMP12 accumulation than in WT→WT mice (Figures 6W and 6X). In tumors, matrix remodeling and MMPs offer new paths for migration and invasion but also allow the release of growth factors that otherwise would remain bound to matrix components, the cell surface, or sequestered by growth factor binding proteins (Bergers et al., 2000; Mott and Werb, 2004). Consistent with this notion, our next observations revealed that soluble versus matrix-bound VEGFC and VEGFD ratios (main lymphangiogenic growth factors) were much lower in *ex vivo* cultured *Pdpn* KO TAMs than in WT TAMs (despite comparable protein levels in WT and KO TAM extracts or in whole tumors from WT→WT and KO→WT mice) (Figures 6Y, 6Z, and S7A–S7D). This suggests that the chemoattractant capacity of these growth factors (and possibly of many others) is reduced in KO→WT mice, as impaired matrix remodeling makes them poorly available in solution. Furthermore, deletion of *Pdpn* in TAMs (and the specific phenotype related to this deletion) did not impinge on the maturation process of exogenous pro-VEGFC (e.g., released by CAFs) into active VEGFC, as assessed by the survival assay of Ba/F3 cells expressing the VEGFR3/EpoR chimera (which require mature VEGFC in order to survive) (Achen et al., 2000) cultured in media derived from immortalized breast CAFs and WT or *Pdpn* KO TAMs (Figure S7E).

To assess if the transcriptional regulation of MMPs and type I collagens depended on GAL8, we analyzed PoEMs, non-PoEMs, and total TAMs isolated from *Lgals8* total KO mice, thus preventing any interaction between PDPN and GAL8 *in vivo*. Under these conditions, we could still appreciate the upregulation of *Mmp9*, *Mmp12*, *Mmp13*, *Col1a1*, and *Col1a2* in PoEMs versus non-PoEMs, whereas the absence of GAL8 did not influence this expression pattern (Figures S7F–S7K). (Lymph)angiogenic genes, i.e., *Vegfa*, *Vegfc*, and *Vegfd*, were instead comparable in all sorted populations, suggesting that neither PDPN nor GAL8 was impacting on their transcription levels (Figures S7L–S7N). Overall, PDPN in TAMs appear to be not only instrumental for favoring the proximity of PoEMs to tumor LVs, but it also regulates the ECM turnover by enhancing collagen formation and degradation. Hence, PoEMs promote lymphangiogenesis and lymphoinvasion both directly by remodeling the matrix in the proximity of growing tumor LVs and indirectly by favoring growth factor liberation and accessibility.

Potential Clinical Relevance of PoEMs in Breast Cancer Patients

Finally, we translated these findings to human breast cancer patients. Similar to murine tumors, 30% of the TAMs expressed PDPN (as assessed in a small cohort of patients) (Figure 7A). Furthermore, freshly sorted human PoEMs, but not non-PoEMs, carried the ability to migrate toward soluble GAL8 (Figure 7B). Likewise, human monocyte-derived PDPN$^+$ macrophages had an enhanced ability to migrate toward LECs, as compared to non-PoEMs (Figure 7C). This migratory capability was lost when LECs were silenced for *LGALS8*. Finally, we analyzed tumor samples from a unique cohort of patients with bilateral synchronous breast tumors, in which one tumor was LN positive (N+), while the contralateral tumor was LN negative (N0). Adhesion of PDPN$^+$ TAMs to the lymphatic walls correlated with the presence of metastasized regional tumor LNs (p value range = 0.00037–0.049). In patients with bilateral tumors that were both N0, we could not observe differences in the number of PDPN$^+$ TAMs interacting with the LV walls (Figures 7D–7F). The total number of infiltrating TAMs did not significantly differ between the N0 and N+ tumors (Figure 7G). When analyzing the N+ subgroup only, patients with both LN and organ metastasis (N+ and M+) had significantly higher numbers of PoEMs per tumor LV than patients with LN metastasis but no organ

(N–P) qRT-PCR analysis of the expression of different vascular endothelial growth factors in CD11b$^+$, F4/80$^+$ TAM populations sorted from 4T1 tumors: PoEMs (PDPN$^+$), non-PoEMs (PDPN$^-$), the total WT TAM pool, and the total *Pdpn* KO TAM pool (PDPN$^-$).

(Q and R) Representative images (Q) and quantifications (R) of collagen I deposition (on the decellularized matrix) by sorted 4T1 TAMs cultured *ex vivo* for 72 h, as assessed by immunofluorescence (IF).

(S and T) Quantifications (S) and representative images (T) of Collagen I deposition around VEGFR3$^+$ lymphatics in 4T1 tumors. The collagen I$^+$ areas were normalized per VEGFR3$^+$ LV area in each field.

(U) Quantification of collagen I digestion by different 4T1 TAM populations cultured *ex vivo* for 72 h, as assed by ELISA recognizing CTX-1 peptide in culture supernatants. The CTX-1 antigen concentrations were normalized versus the mean concentration detected in the WT pool group. CTX-1, type I collagen cross-linked C-telopeptide.

(V) Quantification of gelatin digestion by different 4T1 TAM populations cultured *ex vivo* for 72 h, as assessed spectrophotometrically with the use of direct-quenched (DQ), fluorescein-labeled gelatin. The presence of green fluorescence (indicating proteolytic digestion) was assessed in culture supernatants at 485 nm.

(W and X) Quantifications (W) and representative images (X) of the MMP12$^+$ areas around VEGFR3$^+$ LVs in 4T1 tumors.

(Y and Z) Quantification of VEGFC (Y) and VEGFD (Z) produced by 4T1 TAMs cultured *ex vivo* for 72 h on gelatin, as assessed by ELISA. The data are shown as the ratios of VEGFC or VEGFD concentrations in supernatants (soluble) versus in gelatin (matrix bound). VEGFC, vascular endothelial growth factor C; VEGFD, vascular endothelial growth factor D.

Statistical analysis: *$p < 0.05$; **$p < 0.005$; ***$p < 0.0005$; ****$p < 0.00005$. Graphs show mean ± SEM. Scale bars, 20 μm (Q, T, and X).

IF, immunofluorescence; PoEMs, podoplanin-expressing macrophages; non-PoEMs, podoplanin-negative macrophages; DAPI, 49,6-diamidino-2-phenylindole.

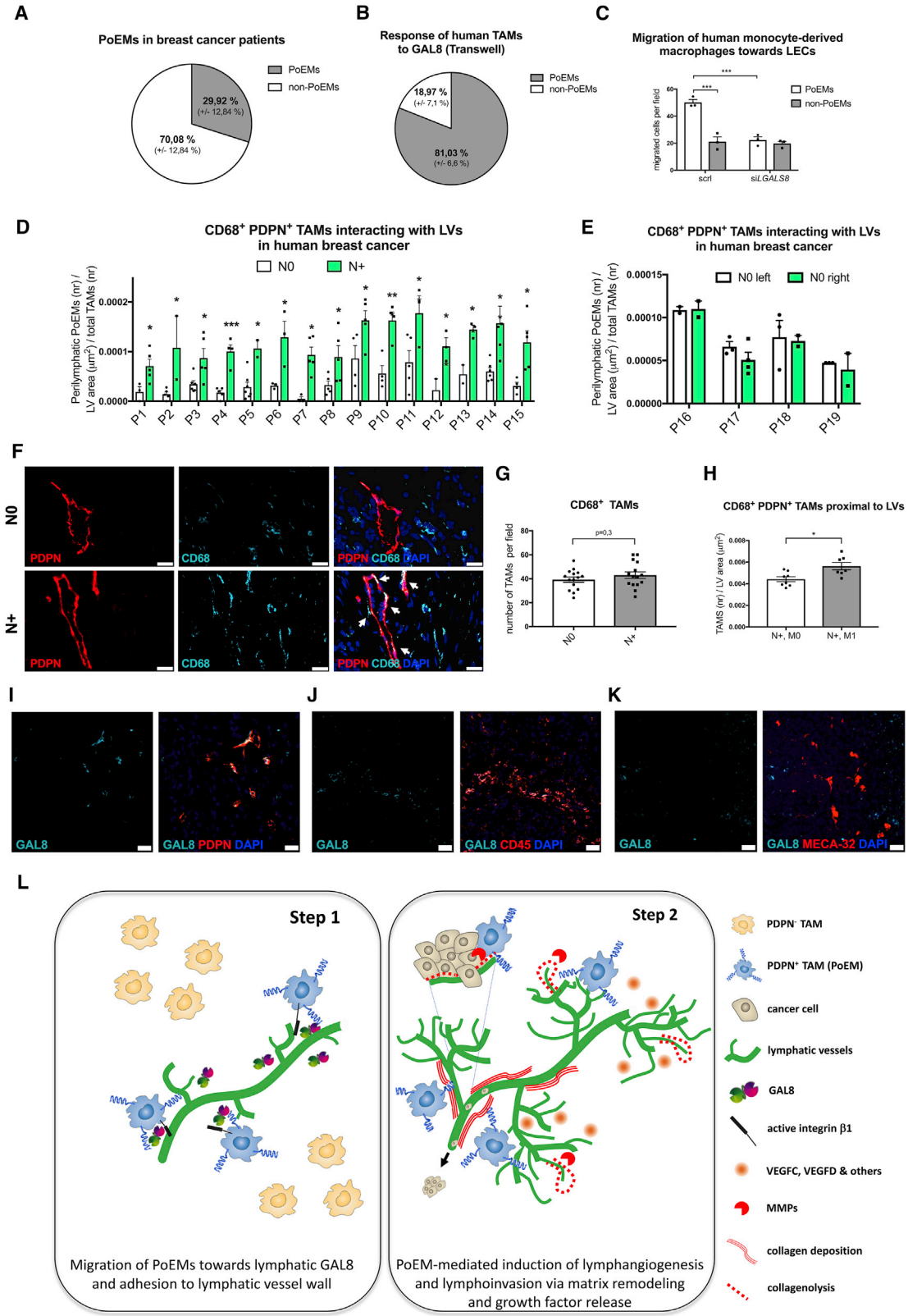

Figure 7. Prospective Clinical Relevance of PoEMs in Breast Cancer Patients

(A) FACS analysis of PDPN in human breast cancer macrophages (CD11b$^+$, CD14$^+$, and HLA-DR$^+$), representing the fraction of PoEMs out of total TAMs.

(B) Quantification of PDPN$^+$ cells (IF) among CD11b$^+$, CD14$^+$, and HLA-DR$^+$ TAMs (sorted from human breast tumor specimens), which have migrated through 8 μm pores (transwell) toward murine recombinant GAL8 (0.5 μM).

(legend continued on next page)

metastasis (N+ and M0) (Figure 7H). Of note, in human breast tumors, GAL8 was expressed by LVs (Figure 7I) and by some infiltrating immune cells (Figure 7J), but not by blood vessels (Figure 7K), mirroring the expression pattern found in murine 4T1 tumors (Figures 3A–3C). These data represent a proof of concept of PoEMs as a potential prognostic marker in breast cancer patients. All together, we demonstrate that PoEMs are present in murine and human breast cancer and that because of their response to LEC-derived GAL8, they localize in direct proximity to tumor lymphatics. Once there, PoEMs locally remodel the ECM and promote lymphangiogenesis and cancer cell lymphoinvasion (Figure 7L).

DISCUSSION

The general understanding on how macrophages influence lymphangiogenesis pinpoints to their production and release of growth factors and metalloproteases (Mantovani, 2010; Noël et al., 2008). However, the mechanisms whereby TAMs interact and participate in the formation of lymphatic conduits within the tumor as well as their impact on cancer cell lymphoinvasion, are not well understood. One of the recently identified mechanisms suggests integrin β4 as the molecule retaining a minor fraction of tumor-educated BMDMs or macrophage-like transformed cells proximal to the tumor lymphatic endothelium when injected systemically during tumor development. Those macrophages stimulate LEC contraction and remodeling via the release of TGF-β1, which could have implications for lymphatic metastasis (Evans et al., 2019). On the other hand, we demonstrate here that PDPN in TAMs engages β1 integrin during the recruitment and adhesion of these cells to GAL8-expressing lymphatics. Once in the perilymphatic space, PoEMs promote ECM remodeling (independently of GAL8 binding), enhancing lymphangiogenesis and metastasis in both a direct (by stimulating lymphatic growth and cancer cell intravasation) and indirect way (through the liberation of VEGFC and VEGFD from the matrix). Specifically, PDPN defines the localization of TAMs around the lymphatic sprouts, but it is also instrumental for matrix remodeling through the transcriptional regulation of MMPs and collagens. As GAL8 induces macrophage migration toward lymphatics but does not impact the expression of ECM-related genes, this transcriptional regulation depends on PDPN but not GAL8. Hence, we speculate that PDPN expression per se is sufficient to induce the translocation of certain transcriptional factors into the nucleus. For example, human pleural mesothelioma cells with high levels of PDPN display active, nuclear YAP1; conversely, PDPN inhibition prevents YAP1 activation (Takeuchi et al., 2017). Consistently, YAP1 has already been described as a transcriptional regulator of collagen (especially type I collagen) and MMPs (Kegelman et al., 2018; Nukuda et al., 2015). Alternatively, another PDPN interactor might be responsible for the regulation of these transcriptional cascades. Vice versa, we cannot exclude that GAL8 is enhancing MMP activity post-transcriptionally and independently of PDPN, for example, through its physical interaction with pro-MMP9 (Nishi et al., 2003) or indirectly, through transactivation of EGFR signaling in other cells, e.g., cancer cells (Oyanadel et al., 2018).

Upon stimulation with GAL8, PDPN in LECs activates VEGFC/VEGFR3-dependent and -independent signals through in *cis* clustering of α1β1/α5β1 integrins (Chen et al., 2016). By using two models of corneal lymphangiogenesis, i.e., allogenic corneal transplantation and HSV infection, this previous study has indicated that global *Lgals8* KO and *Pdpn* KO mice display defective lymphatic sprouting in response to VEGFC. As indicated by *in vitro* assays and *in vivo* cornea stainings, in some physiopathological conditions GAL8 is exclusively expressed by inflammatory cells and binds to PDPN on the LVs. Our study further reveals that in mouse and human tumors, GAL8-expression by the lymphatic endothelium activates in *trans* β1 integrin and PDPN, the latter specifically induced in TAMs by the TME. Our experimental setting with reconstituted GAL8 WT BM in GAL8-deficient hosts allows us to exclude that GAL8 produced by inflammatory cells is the underlying cause of β1 integrin activation in PoEMs. On the other hand, we cannot completely exclude that the "presentation" of GAL8 by the lymphatic endothelium is also due to the cross binding of GAL8 derived from other cells, even though *in vitro* silencing of GAL8 in LECs was sufficient to prevent macrophage adhesion and migration.

In lymphangiogenesis, ECM remodeling is of high importance as, in contrast to BECs (that lean on a basement membrane), LECs are in direct contact with the interstitial matrix and lack (or have an incomplete) basement membrane. Hence, matrix formation and degradation, as well as matrix stiffness, mechanically modulate the ability of cancer cells to migrate and invade LVs. Furthermore, ECM remodeling, or MMPs in general, increase the release of several growth factors (such as VEGF, HGF, FGF, IGF, and others), promoting their chemoattractant potential on neighboring cells, e.g., cancer cells and LECs (Mott and Werb, 2004; Bergers et al., 2000). Here, we show that proximity and adhesion of PoEMs to the lymphatics correlates with matrix remodeling and reorganization enforced by a local production of MMPs and collagens. Despite the fact that

(C) Quantification of the migration of human monocyte-derived macrophages ($CD11b^+$ and $CD14^+$) through 8 μm pores (transwell) in response to soluble factors released by HMVECs. LECs were silenced (si*Lgals8*) or not silenced (scrl) for *Lgals8*, a gene encoding GAL8.

(D–H) IF analysis of $CD68^+$, $PDPN^+$ TAMs interacting with $PDPN^+$ LVs (D–F) or total $CD68^+$ TAMs (G) in paraffin-embedded human breast cancer samples obtained from patients with bilateral tumors, where N0 indicates lack and N+ presence of lymph node metastasis. In N+ positive tumors, the number of $CD68^+$, $PDPN^+$ TAMs interacting with $PDPN^+$ LVs was subsequently correlated with the presence of distant organ metastasis (H).

(I–K) Representative images of human breast tumor sections stained for GAL8 and PDPN (I), GAL8 and CD45 (J), and GAL8 and MECA-32 (K).

(L) In breast cancer, PDPN-expressing macrophages (PoEMs) represent 30% of the entire TAM population. Because of the highest expression of galectin 8 (GAL8) by the lymphatic vessels, PoEMs selectively migrate and interact with the lymphatic endothelium by means of PDPN expression. Binding of GAL8 to PDPN unleashes the clustering and activation of integrin β1, which is required for the chemotactic attraction and adhesion of PoEMs to lymphatic walls. Once there, PoEMs favor lymphangiogenesis via matrix remodeling and the growth factors release. Next, they assist the intravasation of cancer cells into the lymphatic circulation, directly promoting tumor metastasis. Targeting PDPN on macrophages or GAL8 on the lymphatics efficiently impairs this cascade.

Statistical analysis: $^*p < 0.05$; $^{**}p < 0.005$; $^{***}p < 0.0005$. Graphs show mean ± SEM. Scale bar, 20 μm (F and I–K).

PoEMs, podoplanin-expressing macrophages; IF, immunofluorescence; N0, lymph node negative; N+, lymph node positive; P, patient; scrl, scrambled control.

other stromal cells could have higher proteolytic activity than PDPN$^+$ TAMs (as for example tumor-associated neutrophils) or produce a higher extent of collagens (as CAFs), GAL8/integrin β1-mediated adhesion of PoEMs to the LV wall creates a topographic distribution of matrix-remodeling enzymes and enriches the perilymphatic niche with active lymphangiogenic and growth factors. It follows that relocating TAMs out of the perilymphatic space by knocking out *Pdpn* will likely not affect the overall levels of proteases, matrix bundles, and growth factors in the tumor, but it will rather result in a lower concentration of all these proteins around LVs. In contrast, we show that PoEMs are adjacent to LVs but do not integrate into the vessel wall, at least in murine models of breast cancer. Overall, these data support the idea that changes in specific tumor niches can affect cancer progression and therapeutic outcomes (Casazza et al., 2013; Stockmann et al., 2008).

Because of the high upregulation of various collagen subunits and MMPs by PoEMs versus non-PoEMs, the properties of ECM around tumor LVs differ between WT and *Pdpn* KO chimeras. It has been well recognized that the deregulation of ECM is a hallmark of cancer and a factor promoting dissemination (Jena and Janjanam, 2018). Specifically, during breast cancer development, collagen I stiffens the ECM, which promotes tumor invasion and metastasis (Conklin et al., 2011; Zhu et al., 2014). Furthermore, collagen I accelerates lymphatic regeneration and wound repair, supporting its role in the control of lymphatic function (Clavin et al., 2008). Collagen I fiber density was also found to be increased in LN-positive breast cancers (Kakkad et al., 2012). Moreover, various members of the MMP family were identified as poor prognosis markers for breast cancer patients (Radisky and Radisky, 2015). MMPs directly facilitate cancer dissemination by degrading the basement membrane. They can also directly impact cancer cells, releasing growth factors and suppressing apoptosis (Gialeli et al., 2011). Importantly, MMP-mediated blood and lymph vessel formation and generation of tissue disruptive fibrotic stroma provides routes for the spreading of breast cancer (Kessenbrock et al., 2010). Finally, MMPs can directly induce epithelial-mesenchymal transition in breast cancer cells (Nisticò et al., 2012; Radisky and Radisky, 2010).

Tumor lymphangiogenesis requires high levels of energy and creates a unique metabolic milieu. In general, LECs are exposed to high concentrations of glucose, protein, and triglycerides. On the other hand, oxygen concentration in the lymphatic fluid is relatively low, e.g., as compared to arterial blood (Lee et al., 2018). Furthermore, hypoxia drives multiple signaling mechanisms actively involved in lymphangiogenesis and lymphatic metastasis (Ji, 2014). In line with these observations, LECs have been shown to use glycolysis as the main ATP source (85%), with almost inactive mitochondrial glucose oxidation (De Bock et al., 2013). Besides, LECs utilize fatty acids or ketone bodies for acetyl-CoA synthesis in order to sustain the Krebs cycle and dNTP synthesis, along with the production of anaplerotic substrates (García-Caballero et al., 2019; Wong et al., 2017). In our previous study on REDD1$^+$ macrophages, we described a TAM population with a low glycolytic rate, sparing glucose in favor of the blood vascular network (where glucose promotes BEC activation and tumor blood vessel abnormalities) (Wenes et al., 2016). Hence, we can speculate that in a similar fashion, PoEMs—a subset of TAMs adjacent to LVs—might acquire specific metabolic properties in response to their local environment and install a metabolic symbiosis with LECs. Indeed, RNA-seq analysis on PoEMs versus non-PoEMs revealed an upregulation of genes involved in glucose uptake and anaerobic glycolysis in PoEMs. The upregulated transcripts included glucose transporter *Glut1* (*Slc2a1*) (FDR = 2.4×10^{-12}) and multiple glycolytic enzymes, e.g., hexokinase 1 (*Hk1*) (FDR = 4.7×10^{-8}), *Hk2* (FDR = 4.5×10^{-6}), *Hk3* (FDR = 48.8×10^{-19}), aldolase A (*Aldoa*) (FDR = 5.3×10^{-6}), and lactate dehydrogenase (*Ldha*) (FDR = 4.08×10^{-8}). The latter enzyme is responsible for the generation of lactate from pyruvate, which is one of the hallmarks of tumor metabolism (Seth et al., 2017), promoting angiogenesis, immune escape, cell migration, metastasis, and tumor self-sufficiency (San-Millán and Brooks, 2017). In line with this notion, PoEMs upregulated monocarboxylate transporters essential for lactate exchange, e.g., *Mct1* (*Slc16a1*) (FDR = 0.0025) and *Mct4* (*Slc16a3*) (FDR = 7.9×10^{-6}). On the other hand, pyruvate dehydrogenase (*Pdha1*), which encodes an enzyme converting pyruvate to acetyl-CoA during glucose oxidation, was not differentially regulated between PoEMs versus non-PoEMs. Of note, high glycolysis rate in PoEMs might be associated with their high demand for sugar precursors to sustain anabolic metabolism. The increased levels of *Hk1*, *Hk2*, and *Hk3* in PoEMs suggest the flux of the pentose phosphate pathway (PPP) by providing high levels of phosphorylated glucose. By exploiting the oxidative branch of the PPP, PoEMs could provide NADPH for glutathione homeostasis (Samanta and Semenza, 2017). Glutathione is the mainstay of the endogenous anti-oxidative defense system, counteracting reactive oxygen species and sustaining cell functions under hypoxic conditions (Ogunrinu and Sontheimer, 2010). On the other hand, the non-oxidative branch of the PPP provides ribose 5-phosphate, which is necessary for the generation of activated monosaccharides—the building blocks for post-translational protein glycosylation (Carvalho-Cruz et al., 2018; Stincone et al., 2015). For instance, the extracellular domain of PDPN is heavily O-glycosylated, which is a pre-requisite for its interaction with other proteins, e.g., with GAL8 (Troncoso et al., 2014). Likewise, PoEMs upregulate *Colgalt1* (FDR = 0.00059), an enzyme catalyzing the addition of galactose to the hydroxyl groups on collagens I–V, ensuring their proper stiffness, organization, and function (Geister et al., 2019).

In two different mouse models of breast cancer, a subset of TAMs, namely TEMs (TIE2$^+$ TAMs), has been shown to favor hematogenous metastasis by promoting vascular hyper-permeability and cancer cell dissemination in both pre-malignant lesions and late carcinomas (Harney et al., 2015; Linde et al., 2018). Analogically, here, we identify and characterize a subset of TAMs, namely PoEMs that is relevant for lymphoinvasion—the main dissemination route in human TNBC (Mohammed et al., 2011). Our study shows that the presence of PDPN on a specific TAM subset is important for (1) selective macrophage attachment to the lymphatic wall and not the blood vessel wall, (2) LV growth and lymphatic dissemination (via formation of triads of LECs, TAMs, and cancer cells), likely due to (3) increased matrix remodeling per se and, indirectly, by (4) enhancing growth factor liberation and accessibility. The remodeled ECM, as well as a bunch of various growth factors that are virtually liberated by PoEMs, do not necessarily originate from

PoEMs themselves but can be initially produced by other stromal cells, immune cells, or cancer cells.

PoEMs are barely found in normal skin or in wounded corneas. This is in line with a study in breast cancer patients, showing that TEMs in tumors but not in adjacent normal tissues express specific lymphatic markers including PDPN (Bron et al., 2016). Comparable to what has been shown for TIE2 in TEMs, we demonstrate here that PDPN (originally a lymphatic lineage marker) is responsible for the adhesion of a TAM fraction to the tumor lymphatic endothelium. In spite of the similarities between TEMs and PoEMs, our RNA-seq analysis of end-stage 4T1 breast tumors indicates that neither PoEMs nor non-PoEMs express detectable levels of *Tie2/Tek*. Similarly, the transcripts of integrin β4, historically reported to be expressed by epithelial cells (Fuchs et al., 1997), Schwann cells (Einheber et al., 1993), and some subsets of endothelial and smooth muscle cells (Cremona et al., 1994; Kennel et al., 1992; Welser-Alves et al., 2013), were very low in both PDPN-positive and -negative TAMs (77 *Itgb4* transcripts versus 8628 *Itgb1* transcripts), suggesting that the recently described mechanism of macrophage adhesion to lymphatics is not important in our experimental models (Evans et al., 2019).

Unlike VEGFC, which plays an essential role in lymphatic homeostasis as well as in physiological and pathological angiogenesis, the pathway we describe in this study may hold specificity for tumor lymphangiogenesis, therefore circumventing possible side effects (such as lymphoedema) observed in patients and mice treated with anti-VEGFC or anti-VEGFR3 antibodies. Moreover, PDPN-targeted therapies embrace the opportunity to block multiple other cell types and biological processes in cancer, such as the interaction of CAFs with cancer cells (Shindo et al., 2013), dendritic cell trafficking (Acton et al., 2012), collective migration of cancer cells (Shen et al., 2010), and regulatory T cell development and T cell exhaustion (Fuertbauer et al., 2013). We also validate that genetic or pharmacologic blockade of GAL8 prevents PoEM proximity to the LVs, thus reducing tumor lymphangiogenesis and metastatic dissemination. These observations pave the way toward the screening and the use of PDPN- and GAL8-specific inhibitors or blocking antibodies in cancer therapy. Even more clinically relevant, the analysis of PoEMs in a tumor could be an indication for complete LN resection or for adjuvant chemotherapy. Larger cohorts of patients are warranted to further explore this idea.

Limitations of Study

PoEMs stimulate lymphangiogenesis and lymphatic dissemination in murine and human breast cancer. It remains to be investigated whether PoEMs are present in other tumor types and whether they play there a similar role as in breast cancer. It follows that bivalent-blocking antibodies targeting PDPN specifically in TAMs (or improved and specific inhibitors of GAL8) could constitute an advantageous anti-metastatic strategy. However, the next challenges toward this direction are (1) to identify the domains that need to be blocked to achieve this goal (i.e., the GAL8 binding site versus the CLEC2 binding site) and (2) to understand how the presence of glycosylic groups in both PDPN and GAL8 is limiting for their physical interaction, and thus has to be taken into account in the design of blocking agents. Furthermore, our findings underpin the possibility to generate *in vitro* PoEMs in order to enable lymphangiogenesis and lymphatic drainage in case of lymphedema, which occurs in many pathological conditions, including obesity, infections, or congenital diseases. Aligned with a role of PoEMs in contexts other than cancer, we still do not know the physiology underlying the existence of PoEMs: our GO analysis suggests that PoEMs might be involved in the repair of hepatic wounds where their dysregulation may lead to liver fibrosis. Finally, the transcriptomic differences between PoEMs and non-PoEMs, suggesting their distinctive metabolic profiles, should be further explored, possibly resulting in "metabolic reprogramming" therapies that could reduce PoEM-induced lymphangiogenesis.

STAR★METHODS

Detailed methods are provided in the online version of this paper and include the following:

- KEY RESOURCES TABLE
- LEAD CONTACT AND MATERIALS AVAILABILITY
- EXPERIMENTAL MODEL AND SUBJECT DETAILS
  - Animals
  - Cell Lines
  - Cell Isolation and Culture
  - Breast Cancer Patients
- METHOD DETAILS
  - Assessment of LEC Identity, Proliferation and Apoptosis
  - Assessment of Intercellular GAPs in LEC Monolayers
  - Ba/F3 Viability Assay
  - BMDM-LEC Adhesion Assay
  - Bone Marrow Transplantation
  - Collagen I Degradation by 4T1 TAMs Ex Vivo
  - Corneal Cauterization Assay
  - FACS Analysis and Flow Sorting of Human TAMs
  - FACS Analysis and Flow Sorting of Murine Tissue- and Tumor-Infiltrating Leukocytes
  - Gelatin Degradation by 4T1 TAMs Ex Vivo
  - Gene Silencing *In Vitro*
  - Histology and Immunostainings
  - Immunofluorescence in BMDMs
  - Immunofluorescence in Sorted TAMs
  - Injection of 4T1 Cancer Cells into Lymph Nodes
  - Intratumoral Thiodigalactoside (TDG) Treatment
  - Intratumoral VEGFR3-Blocking Antibody Treatment
  - LEC Capillary-like Structure Formation Assay
  - Lgals8 Overexpression in LECs
  - Lung Colonization Assay
  - Lymphangiography
  - Macrophage Migration Assays
  - Metastatic Tumor Models
  - PDPN-Integrin β1 Co-immunoprecipitation
  - Perilymphatic TAMs
  - Proximity Ligation Assay (PLA)
  - qRT-PCR
  - RNA Sequencing
  - Spheroid LEC Sprouting Assay
  - Three-Dimensional Reconstructions of TAM-Lymphatic Vessel-Cancer Cell Triads

SUPPLEMENTAL INFORMATION

Supplemental Information can be found online at https://doi.org/10.1016/j.cmet.2019.07.015.

ACKNOWLEDGMENTS

We thank Jens Serneels, Mateusz Antoszewski, Sander Willox, and Eline Achten for technical support and Prof. Ghislain Opdenakker and Prof. Michele De Palma for their expert advice. This work was supported by a European Research Council (ERC) Consolidator - grant (773208; EU), by Worldwide Cancer Research (13-1031; United Kingdom), and by Fonds Wetenschappelijk Onderzoek (FWO) (G087615N; Belgium). R.M.-P. is funded by FWO and M.E. by Kom op Tegen Kanker (Stand up to Cancer), a Flemish Cancer Research Foundation. M.M. received long-term structural Methusalem funding by the Flemish government (METH.14.08).

AUTHOR CONTRIBUTIONS

P.B.-K. performed the experimental design, all experiments, data acquisition, and interpretation. R.M.-P. performed the *in vitro* assays and FACS analysis. M.E. performed the tumor experiments, confocal stainings, and analysis. M.G.-C. performed the corneal wound assays and spheroid sprouting assays. S. Pinioti and S. Pretto performed the stainings, quantifications, and cell sorting. R.K. assisted in all the experimental work. C.A. performed the tumor experiments and helped in generating the *Pdpn* floxed mice. M.D.M. performed all the cloning and viral preparations. H.P., A.S., and G.F. provided all the clinical samples and information. G.F. also evaluated the mouse tissues. M.V.T. and O.C. provided the *Lgals8* KO mice. J.A.V.G. and P.B.-K. helped in writing the manuscript. J.A.V.G. also helped with FACS. M.M. performed the experimental design, data analysis, conducted the scientific direction, and wrote the manuscript.

DECLARATION OF INTERESTS

M.M. and P.B.-K. are named inventors on a patent application claiming subject matter related to the results described in this paper (EP 17198684.7). The other authors declare no competing interests.

Received: June 13, 2019
Revised: July 5, 2019
Accepted: July 29, 2019
Published: August 22, 2019

REFERENCES

Achen, M.G., Roufail, S., Domagala, T., Catimel, B., Nice, E.C., Geleick, D.M., Murphy, R., Scott, A.M., Caesar, C., Makinen, T., et al. (2000). Monoclonal antibodies to vascular endothelial growth factor-D block its interactions with both VEGF receptor-2 and VEGF receptor-3. Eur. J. Biochem. *267*, 2505–2515.

Acton, S.E., Astarita, J.L., Malhotra, D., Lukacs-Kornek, V., Franz, B., Hess, P.R., Jakus, Z., Kuligowski, M., Fletcher, A.L., Elpek, K.G., et al. (2012). Podoplanin-rich stromal networks induce dendritic cell motility via activation of the C-type lectin receptor CLEC-2. Immunity *37*, 276–289.

Astarita, J.L., Acton, S.E., and Turley, S.J. (2012). Podoplanin: emerging functions in development, the immune system, and cancer. Front. Immunol. *3*, 283.

Ayoub, J.P., Verma, Sh, and Verma, S. (2012). Advances in the management of metastatic breast cancer: options beyond first-line chemotherapy. Curr. Oncol. *19*, 91–105.

Barcus, C.E., O'Leary, K.A., Brockman, J.L., Rugowski, D.E., Liu, Y., Garcia, N., Yu, M., Keely, P.J., Eliceiri, K.W., and Schuler, L.A. (2017). Elevated collagen-I augments tumor progressive signals, intravasation and metastasis of prolactin-induced estrogen receptor alpha positive mammary tumor cells. Breast Cancer Res. *19*, 9.

Bergers, G., Brekken, R., McMahon, G., Vu, T.H., Itoh, T., Tamaki, K., Tanzawa, K., Thorpe, P., Itohara, S., Werb, Z., et al. (2000). Matrix metalloproteinase-9 triggers the angiogenic switch during carcinogenesis. Nat. Cell Biol. *2*, 737–744.

Braun, M., Flucke, U., Debald, M., Walgenbach-Bruenagel, G., Walgenbach, K.J., Höller, T., Pölcher, M., Wolfgarten, M., Sauerwald, A., Keyver-Paik, M., et al. (2008). Detection of lymphovascular invasion in early breast cancer by D2-40 (podoplanin): a clinically useful predictor for axillary lymph node metastases. Breast Cancer Res. Treat. *112*, 503–511.

Braun, A., Worbs, T., Moschovakis, G.L., Halle, S., Hoffmann, K., Bölter, J., Münk, A., and Förster, R. (2011). Afferent lymph-derived T cells and DCs use different chemokine receptor CCR7-dependent routes for entry into the lymph node and intranodal migration. Nat. Immunol. *12*, 879–887.

Bron, S., Henry, L., Faes-Van't Hull, E., Turrini, R., Vanhecke, D., Guex, N., Ifticene-Treboux, A., Marina Iancu, E., Semilietof, A., Rufer, N., et al. (2016). TIE-2-expressing monocytes are lymphangiogenic and associate specifically with lymphatics of human breast cancer. Oncoimmunology *5*, e1073882.

Carabelli, J., Quattrocchi, V., D'Antuono, A., Zamorano, P., Tribulatti, M.V., and Campetella, O. (2017). Galectin-8 activates dendritic cells and stimulates antigen-specific immune response elicitation. J. Leukoc. Biol. *102*, 1237–1247.

Carvalho-Cruz, P., Alisson-Silva, F., Todeschini, A.R., and Dias, W.B. (2018). Cellular glycosylation senses metabolic changes and modulates cell plasticity during epithelial to mesenchymal transition. Dev. Dyn. *247*, 481–491.

Casazza, A., Laoui, D., Wenes, M., Rizzolio, S., Bassani, N., Mambretti, M., Deschoemaeker, S., Van Ginderachter, J.A., Tamagnone, L., and Mazzone, M. (2013). Impeding macrophage entry into hypoxic tumor areas by Sema3A/Nrp1 signaling blockade inhibits angiogenesis and restores antitumor immunity. Cancer Cell *24*, 695–709.

Chelluboina, B., Warhekar, A., Dillard, M., Klopfenstein, J.D., Pinson, D.M., Wang, D.Z., and Veeravalli, K.K. (2015). Post-transcriptional inactivation of matrix metalloproteinase-12 after focal cerebral ischemia attenuates brain damage. Sci. Rep. *5*, 9504.

Chen, W.S., Cao, Z., Sugaya, S., Lopez, M.J., Sendra, V.G., Laver, N., Leffler, H., Nilsson, U.J., Fu, J., Song, J., et al. (2016). Pathological lymphangiogenesis is modulated by galectin-8-dependent crosstalk between podoplanin and integrin-associated VEGFR-3. Nat. Commun. *7*, 11302.

Clark, A.G., and Vignjevic, D.M. (2015). Modes of cancer cell invasion and the role of the microenvironment. Curr. Opin. Cell Biol. *36*, 13–22.

Clavin, N.W., Avraham, T., Fernandez, J., Daluvoy, S.V., Soares, M.A., Chaudhry, A., and Mehrara, B.J. (2008). TGF-beta1 is a negative regulator of lymphatic regeneration during wound repair. Am. J. Physiol. Heart Circ. Physiol. *295*, H2113–H2127.

Conklin, M.W., Eickhoff, J.C., Riching, K.M., Pehlke, C.A., Eliceiri, K.W., Provenzano, P.P., Friedl, A., and Keely, P.J. (2011). Aligned collagen is a prognostic signature for survival in human breast carcinoma. Am. J. Pathol. *178*, 1221–1232.

Cremona, O., Savoia, P., Marchisio, P.C., Gabbiani, G., and Chaponnier, C. (1994). The alpha 6 and beta 4 integrin subunits are expressed by smooth muscle cells of human small vessels: a new localization in mesenchymal cells. J. Histochem. Cytochem. *42*, 1221–1228.

Cueni, L.N., Hegyi, I., Shin, J.W., Albinger-Hegyi, A., Gruber, S., Kunstfeld, R., Moch, H., and Detmar, M. (2010). Tumor lymphangiogenesis and metastasis to lymph nodes induced by cancer cell expression of podoplanin. Am. J. Pathol. *177*, 1004–1016.

De Bock, K., Georgiadou, M., Schoors, S., Kuchnio, A., Wong, B.W., Cantelmo, A.R., Quaegebeur, A., Ghesquière, B., Cauwenberghs, S., Eelen, G., et al. (2013). Role of PFKFB3-driven glycolysis in vessel sprouting. Cell *154*, 651–663.

De Palma, M., and Naldini, L. (2011). Angiopoietin-2 TIEs up macrophages in tumor angiogenesis. Clin. Cancer Res. *17*, 5226–5232.

Detry, B., Bruyère, F., Erpicum, C., Paupert, J., Lamaye, F., Maillard, C., Lenoir, B., Foidart, J.M., Thiry, M., and Noël, A. (2011). Digging deeper into lymphatic vessel formation in vitro and in vivo. BMC Cell Biol. *12*, 29.

Du, R., Lu, K.V., Petritsch, C., Liu, P., Ganss, R., Passegué, E., Song, H., Vandenberg, S., Johnson, R.S., Werb, Z., et al. (2008). HIF1alpha induces the recruitment of bone marrow-derived vascular modulatory cells to regulate tumor angiogenesis and invasion. Cancer Cell *13*, 206–220.

Einheber, S., Milner, T.A., Giancotti, F., and Salzer, J.L. (1993). Axonal regulation of Schwann cell integrin expression suggests a role for alpha 6 beta 4 in myelination. J. Cell Biol. *123*, 1223–1236.

Evans, R., Flores-Borja, F., Nassiri, S., Miranda, E., Lawler, K., Grigoriadis, A., Monypenny, J., Gillet, C., Owen, J., Gordon, P., et al. (2019). Integrin-mediated macrophage adhesion promotes lymphovascular dissemination in breast cancer. Cell Rep. *27*, 1967–1978.

Fuchs, E., Dowling, J., Segre, J., Lo, S.H., and Yu, Q.C. (1997). Integrators of epidermal growth and differentiation: distinct functions for beta 1 and beta 4 integrins. Curr. Opin. Genet. Dev. *7*, 672–682.

Fuertbauer, E., Zaujec, J., Uhrin, P., Raab, I., Weber, M., Schachner, H., Bauer, M., Schütz, G.J., Binder, B.R., Sixt, M., et al. (2013). Thymic medullar conduits-associated podoplanin promotes natural regulatory T cells. Immunol. Lett. *154*, 31–41.

García-Caballero, M., Paupert, J., Blacher, S., Van de Velde, M., Quesada, A.R., Medina, M.A., and Noël, A. (2017). Targeting VEGFR-3/-2 signaling pathways with AD0157: a potential strategy against tumor-associated lymphangiogenesis and lymphatic metastases. J. Hematol. Oncol. *10*, 122.

García-Caballero, M., Zecchin, A., Souffreau, J., Truong, A.K., Teuwen, L., Vermaelen, W., Martín-Pérez, R., de Zeeuw, P., Bouché, A., Vinckier, S., et al. (2019). Role and therapeutic potential of dietary ketone bodies in lymph vessel growth. Nat. Metab. *1*, 666–675.

Garnero, P., Ferreras, M., Karsdal, M.A., Nicamhlaoibh, R., Risteli, J., Borel, O., Qvist, P., Delmas, P.D., Foged, N.T., and Delaissé, J.M. (2003). The type I collagen fragments ICTP and CTX reveal distinct enzymatic pathways of bone collagen degradation. J. Bone Miner. Res. *18*, 859–867.

Geister, K.A., Lopez-Jimenez, A.J., Houghtaling, S., Ho, T.H., Vanacore, R., and Beier, D.R. (2019). Loss of function of Colgalt1 disrupts collagen post-translational modification and causes musculoskeletal defects. Dis. Model Mech. *12*.

Gialeli, C., Theocharis, A.D., and Karamanos, N.K. (2011). Roles of matrix metalloproteinases in cancer progression and their pharmacological targeting. FEBS J. *278*, 16–27.

Harney, A.S., Arwert, E.N., Entenberg, D., Wang, Y., Guo, P., Qian, B.Z., Oktay, M.H., Pollard, J.W., Jones, J.G., and Condeelis, J.S. (2015). Real-time imaging reveals local, transient vascular permeability, and tumor cell intravasation stimulated by TIE2hi macrophage-derived VEGFA. Cancer Discov. *5*, 932–943.

Heiss, M., Hellström, M., Kalén, M., May, T., Weber, H., Hecker, M., Augustin, H.G., and Korff, T. (2015). Endothelial cell spheroids as a versatile tool to study angiogenesis in vitro. FASEB J. *29*, 3076–3084.

Ito, K., Scott, S.A., Cutler, S., Dong, L.F., Neuzil, J., Blanchard, H., and Ralph, S.J. (2011). Thiodigalactoside inhibits murine cancers by concurrently blocking effects of galectin-1 on immune dysregulation, angiogenesis and protection against oxidative stress. Angiogenesis *14*, 293–307.

Jacob, A., Jing, J., Lee, J., Schedin, P., Gilbert, S.M., Peden, A.A., Junutula, J.R., and Prekeris, R. (2013). Rab40b regulates trafficking of MMP2 and MMP9 during invadopodia formation and invasion of breast cancer cells. J. Cell Sci. *126*, 4647–4658.

Jena, M.K., and Janjanam, J. (2018). Role of extracellular matrix in breast cancer development: a brief update. F1000Res. *7*, 274.

Ji, R.C. (2014). Hypoxia and lymphangiogenesis in tumor microenvironment and metastasis. Cancer Lett. *346*, 6–16.

Ji, H., Cao, R., Yang, Y., Zhang, Y., Iwamoto, H., Lim, S., Nakamura, M., Andersson, P., Wang, J., Sun, Y., et al. (2014). TNFR1 mediates TNF-alpha-induced tumour lymphangiogenesis and metastasis by modulating VEGF-C-VEGFR3 signalling. Nat. Commun. *5*, 4944.

Kakkad, S.M., Solaiyappan, M., Argani, P., Sukumar, S., Jacobs, L.K., Leibfritz, D., Bhujwalla, Z.M., and Glunde, K. (2012). Collagen I fiber density increases in lymph node positive breast cancers: pilot study. J. Biomed. Opt. *17*, 116017.

Kegelman, C.D., Mason, D.E., Dawahare, J.H., Horan, D.J., Vigil, G.D., Howard, S.S., Robling, A.G., Bellido, T.M., and Boerckel, J.D. (2018). Skeletal cell YAP and TAZ combinatorially promote bone development. FASEB J. *32*, 2706–2721.

Kennel, S.J., Godfrey, V., Ang, L.Y., Lankford, T.K., Foote, L.J., and Makkinje, A. (1992). The beta 4 subunit of the integrin family is displayed on a restricted subset of endothelium in mice. J. Cell Sci. *101*, 145–150.

Kessenbrock, K., Plaks, V., and Werb, Z. (2010). Matrix metalloproteinases: regulators of the tumor microenvironment. Cell *141*, 52–67.

Laaf, D., Bojarová, P., Elling, L., and Křen, V. (2019). Galectin-carbohydrate interactions in biomedicine and biotechnology. Trends Biotechnol. *37*, 402–415.

Laakkonen, P., Waltari, M., Holopainen, T., Takahashi, T., Pytowski, B., Steiner, P., Hicklin, D., Persaud, K., Tonra, J.R., Witte, L., et al. (2007). Vascular endothelial growth factor receptor 3 is involved in tumor angiogenesis and growth. Cancer Res. *67*, 593–599.

Lee, H.W., Yu, P., and Simons, M. (2018). Recent advances in understanding lymphangiogenesis and metabolism. F1000Res. *7*.

Li, J., Wang, J.J., Peng, Q., Chen, C., Humphrey, M.B., Heinecke, J., and Zhang, S.X. (2012). Macrophage metalloelastase (MMP-12) deficiency mitigates retinal inflammation and pathological angiogenesis in ischemic retinopathy. PLoS One *7*, e52699.

Linde, N., Casanova-Acebes, M., Sosa, M.S., Mortha, A., Rahman, A., Farias, E., Harper, K., Tardio, E., Reyes Torres, I., Jones, J., et al. (2018). Macrophages orchestrate breast cancer early dissemination and metastasis. Nat. Commun. *9*, 21.

Mahtab, E.A., Wijffels, M.C., Van Den Akker, N.M., Hahurij, N.D., Lie-Venema, H., Wisse, L.J., Deruiter, M.C., Uhrin, P., Zaujec, J., Binder, B.R., et al. (2008). Cardiac malformations and myocardial abnormalities in podoplanin knockout mouse embryos: correlation with abnormal epicardial development. Dev. Dyn. *237*, 847–857.

Mantovani, A. (2010). Molecular pathways linking inflammation and cancer. Curr. Mol. Med. *10*, 369–373.

Markowska, A.I., Liu, F.T., and Panjwani, N. (2010). Galectin-3 is an important mediator of VEGF- and bFGF-mediated angiogenic response. J. Exp. Med. *207*, 1981–1993.

Mazzone, M., Dettori, D., de Oliveira, R.L., Loges, S., Schmidt, T., Jonckx, B., Tian, Y.M., Lanahan, A.A., Pollard, P., de Almodovar, C.R., et al. (2009). Heterozygous deficiency of PHD2 restores tumor oxygenation and inhibits metastasis via endothelial normalization. Cell *136*, 839–851.

Meng, F., and Lowell, C.A. (1998). A beta 1 integrin signaling pathway involving Src-family kinases, Cbl and PI-3 kinase is required for macrophage spreading and migration. EMBO J. *17*, 4391–4403.

Mohammed, R.A., Ellis, I.O., Mahmmod, A.M., Hawkes, E.C., Green, A.R., Rakha, E.A., and Martin, S.G. (2011). Lymphatic and blood vessels in basal and triple-negative breast cancers: characteristics and prognostic significance. Mod. Pathol. *24*, 774–785.

Mott, J.D., and Werb, Z. (2004). Regulation of matrix biology by matrix metalloproteinases. Curr. Opin. Cell Biol. *16*, 558–564.

Nielsen, S.R., and Schmid, M.C. (2017). Macrophages as key drivers of cancer progression and metastasis. Mediators Inflamm. *2017*, 9624760.

Nishi, N., Shoji, H., Seki, M., Itoh, A., Miyanaka, H., Yuube, K., Hirashima, M., and Nakamura, T. (2003). Galectin-8 modulates neutrophil function via interaction with integrin alphaM. Glycobiology *13*, 755–763.

Nisticò, P., Bissell, M.J., and Radisky, D.C. (2012). Epithelial-mesenchymal transition: general principles and pathological relevance with special emphasis on the role of matrix metalloproteinases. Cold Spring Harb. Perspect. Biol. *4*.

Noël, A., Jost, M., and Maquoi, E. (2008). Matrix metalloproteinases at cancer tumor-host interface. Semin. Cell Dev. Biol. *19*, 52–60.

Nukuda, A., Sasaki, C., Ishihara, S., Mizutani, T., Nakamura, K., Ayabe, T., Kawabata, K., and Haga, H. (2015). Stiff substrates increase YAP-signaling-mediated matrix metalloproteinase-7 expression. Oncogenesis *4*, e165.

Ogunrinu, T.A., and Sontheimer, H. (2010). Hypoxia increases the dependence of glioma cells on glutathione. J. Biol. Chem. *285*, 37716–37724.

Oyanadel, C., Holmes, C., Pardo, E., Retamal, C., Shaughnessy, R., Smith, P., Cortés, P., Bravo-Zehnder, M., Metz, C., Feuerhake, T., et al. (2018). Galectin-8 induces partial epithelial-mesenchymal transition with invasive tumorigenic capabilities involving a FAK/EGFR/proteasome pathway in Madin-Darby canine kidney cells. Mol. Biol. Cell *29*, 557–574.

Palmieri, E.M., Spera, I., Menga, A., Infantino, V., Porcelli, V., Iacobazzi, V., Pierri, C.L., Hooper, D.C., Palmieri, F., and Castegna, A. (2015). Acetylation of human mitochondrial citrate carrier modulates mitochondrial citrate/malate exchange activity to sustain NADPH production during macrophage activation. Biochim. Biophys. Acta *1847*, 729–738.

Pucci, F., Venneri, M.A., Biziato, D., Nonis, A., Moi, D., Sica, A., Di Serio, C., Naldini, L., and De Palma, M. (2009). A distinguishing gene signature shared by tumor-infiltrating Tie2-expressing monocytes, blood "resident" monocytes, and embryonic macrophages suggests common functions and developmental relationships. Blood *114*, 901–914.

Pulaski, B.A., and Ostrand-Rosenberg, S. (2001). Mouse 4T1 breast tumor model. Curr Protoc Immunol *22*, Chapter 20, Unit 20.

Radisky, E.S., and Radisky, D.C. (2010). Matrix metalloproteinase-induced epithelial-mesenchymal transition in breast cancer. J. Mammary Gland Biol. Neoplasia *15*, 201–212.

Radisky, E.S., and Radisky, D.C. (2015). Matrix metalloproteinases as breast cancer drivers and therapeutic targets. Front. Biosci. (Landmark Ed.) *20*, 1144–1163.

Ran, S., Volk, L., Hall, K., and Flister, M.J. (2010). Lymphangiogenesis and lymphatic metastasis in breast cancer. Pathophysiology *17*, 229–251.

Samanta, D., and Semenza, G.L. (2017). Maintenance of redox homeostasis by hypoxia-inducible factors. Redox Biol. *13*, 331–335.

San-Millán, I., and Brooks, G.A. (2017). Reexamining cancer metabolism: lactate production for carcinogenesis could be the purpose and explanation of the Warburg effect. Carcinogenesis *38*, 119–133.

Schoors, S., Bruning, U., Missiaen, R., Queiroz, K.C., Borgers, G., Elia, I., Zecchin, A., Cantelmo, A.R., Christen, S., Goveia, J., et al. (2015). Fatty acid carbon is essential for dNTP synthesis in endothelial cells. Nature *520*, 192–197.

Seth, P., Csizmadia, E., Hedblom, A., Vuerich, M., Xie, H., Li, M., Longhi, M.S., and Wegiel, B. (2017). Deletion of lactate dehydrogenase-A in myeloid cells triggers antitumor immunity. Cancer Res. *77*, 3632–3643.

Shen, Y., Chen, C.S., Ichikawa, H., and Goldberg, G.S. (2010). SRC induces podoplanin expression to promote cell migration. J. Biol. Chem. *285*, 9649–9656.

Shibuya, M. (2006). Vascular endothelial growth factor receptor-1 (VEGFR-1/Flt-1): a dual regulator for angiogenesis. Angiogenesis *9*, 225–230.

Shindo, K., Aishima, S., Ohuchida, K., Fujiwara, K., Fujino, M., Mizuuchi, Y., Hattori, M., Mizumoto, K., Tanaka, M., and Oda, Y. (2013). Podoplanin expression in cancer-associated fibroblasts enhances tumor progression of invasive ductal carcinoma of the pancreas. Mol. Cancer *12*, 168.

Skobe, M., Hawighorst, T., Jackson, D.G., Prevo, R., Janes, L., Velasco, P., Riccardi, L., Alitalo, K., Claffey, K., and Detmar, M. (2001). Induction of tumor lymphangiogenesis by VEGF-C promotes breast cancer metastasis. Nat. Med. *7*, 192–198.

Stacker, S.A., Williams, S.P., Karnezis, T., Shayan, R., Fox, S.B., and Achen, M.G. (2014). Lymphangiogenesis and lymphatic vessel remodelling in cancer. Nat. Rev. Cancer *14*, 159–172.

Stincone, A., Prigione, A., Cramer, T., Wamelink, M.M., Campbell, K., Cheung, E., Olin-Sandoval, V., Grüning, N.M., Krüger, A., Tauqeer Alam, M., et al. (2015). The return of metabolism: biochemistry and physiology of the pentose phosphate pathway. Biol. Rev. Camb. Philos. Soc. *90*, 927–963.

Stockmann, C., Doedens, A., Weidemann, A., Zhang, N., Takeda, N., Greenberg, J.I., Cheresh, D.A., and Johnson, R.S. (2008). Deletion of vascular endothelial growth factor in myeloid cells accelerates tumorigenesis. Nature *456*, 814–818.

Suzuki, H., Kato, Y., Kaneko, M.K., Okita, Y., Narimatsu, H., and Kato, M. (2008). Induction of podoplanin by transforming growth factor-beta in human fibrosarcoma. FEBS Lett. *582*, 341–345.

Suzuki, H., Onimaru, M., Yonemitsu, Y., Maehara, Y., Nakamura, S., and Sueishi, K. (2010). Podoplanin in cancer cells is experimentally able to attenuate prolymphangiogenic and lymphogenous metastatic potentials of lung squamoid cancer cells. Mol. Cancer *9*, 287.

Swierczak, A., Cook, A.D., Lenzo, J.C., Restall, C.M., Doherty, J.P., Anderson, R.L., and Hamilton, J.A. (2014). The promotion of breast cancer metastasis caused by inhibition of CSF-1R/CSF-1 signaling is blocked by targeting the G-CSF receptor. Cancer Immunol. Res. *2*, 765–776.

Takeuchi, S., Fukuda, K., Yamada, T., Arai, S., Takagi, S., Ishii, G., Ochiai, A., Iwakiri, S., Itoi, K., Uehara, H., et al. (2017). Podoplanin promotes progression of malignant pleural mesothelioma by regulating motility and focus formation. Cancer Sci. *108*, 696–703.

Tejchman, A., Lamerant-Fayel, N., Jacquinet, J.C., Bielawska-Pohl, A., Mleczko-Sanecka, K., Grillon, C., Chouaib, S., Ugorski, M., and Kieda, C. (2017). Tumor hypoxia modulates podoplanin/CCL21 interactions in CCR7+ NK cell recruitment and CCR7+ tumor cell mobilization. Oncotarget *8*, 31876–31887.

Tribulatti, M.V., Figini, M.G., Carabelli, J., Cattaneo, V., and Campetella, O. (2012). Redundant and antagonistic functions of galectin-1, -3, and -8 in the elicitation of T cell responses. J. Immunol. *188*, 2991–2999.

Troncoso, M.F., Ferragut, F., Bacigalupo, M.L., Cárdenas Delgado, V.M., Nugnes, L.G., Gentilini, L., Laderach, D., Wolfenstein-Todel, C., Compagno, D., Rabinovich, G.A., et al. (2014). Galectin-8: a matricellular lectin with key roles in angiogenesis. Glycobiology *24*, 907–914.

Ugorski, M., Dziegiel, P., and Suchanski, J. (2016). Podoplanin - a small glycoprotein with many faces. Am. J. Cancer Res. *6*, 370–386.

Uhrin, P., Zaujec, J., Breuss, J.M., Olcaydu, D., Chrenek, P., Stockinger, H., Fuertbauer, E., Moser, M., Haiko, P., Fässler, R., et al. (2010). Novel function for blood platelets and podoplanin in developmental separation of blood and lymphatic circulation. Blood *115*, 3997–4005.

Welser-Alves, J.V., Boroujerdi, A., Tigges, U., Wrabetz, L., Feltri, M.L., and Milner, R. (2013). Endothelial beta4 integrin is predominantly expressed in arterioles, where it promotes vascular remodeling in the hypoxic brain. Arterioscler. Thromb. Vasc. Biol. *33*, 943–953.

Wenes, M., Shang, M., Di Matteo, M., Goveia, J., Martín-Pérez, R., Serneels, J., Prenen, H., Ghesquière, B., Carmeliet, P., and Mazzone, M. (2016). Macrophage metabolism controls tumor blood vessel morphogenesis and metastasis. Cell Metab. *24*, 701–715.

Wong, B.W., Wang, X., Zecchin, A., Thienpont, B., Cornelissen, I., Kalucka, J., García-Caballero, M., Missiaen, R., Huang, H., Brüning, U., et al. (2017). The role of fatty acid beta-oxidation in lymphangiogenesis. Nature *542*, 49–54.

Zheng, W., Aspelund, A., and Alitalo, K. (2014). Lymphangiogenic factors, mechanisms, and applications. J. Clin. Invest. *124*, 878–887.

Zhu, J., Xiong, G., Trinkle, C., and Xu, R. (2014). Integrated extracellular matrix signaling in mammary gland development and breast cancer progression. Histol. Histopathol. *29*, 1083–1092.

STAR★METHODS

KEY RESOURCES TABLE

REAGENT or RESOURCE	SOURCE	IDENTIFIER
Antibodies		
Alexa Fluor-647 donkey anti-goat IgG	Invitrogen	A21447; RRID: AB_141844
Anti-human CD45	Sino Biological	100342-R145
Anti-human CD68	Dako	M0876; RRID: AB_2074844
Anti-human GAL8	GTX	117687; RRID: AB_11171622
Anti-human MECA-32	GTX	54474
Anti-human PDPN	eBioscience	14-9381-82; RRID: AB_1603307
Anti-mouse CD115-PE/Cy7	BioLegend	135523; RRID: AB_2566459
Anti-mouse CD11b-PE-Cy7	eBioscience	25-0112-81; RRID: AB_469587
Anti-mouse CD11c APC	eBioscience	17-0114-81; RRID: AB_469345
Anti-mouse CD204-APC	Miltenyi Biotec	130-102-285; RRID: AB_2656173
Anti-mouse CD326 (EpCAM) PerCP-eFluor710	eBioscience	46-5791-80; RRID: AB_10597602
Anti-mouse CD8a-APC/Cy7	BioLegend	100714; RRID: AB_312753
Anti-mouse F4/80-FITC	eBioscience	53-4801-82; RRID: AB_469915
Anti-mouse MHC Class II-PE/Cy7	eBioscience	25-5321-80; RRID: AB_10852868
Anti-mouse Pdpn	R&D Systems	AF3244; RRID: AB_2268062
Anti-mouse Podoplanin-APC	BioLegend	127410; RRID: AB_2268062
Anti-mouse/rat CD29 [HMβ1-1]	BioLegend	102202; RRID: AB_312879
Anti-mouse/rat integrin beta 1	R&D Systems	AF2405; RRID: AB_416591
Armenian hamster anti-mouse/rat CD29	BioLegend	102202; RRID: AB_312879
Armenian hamster IgG isotype	BioLegend	400933
Biotin-SP-AffiniPure goat anti-syrian hamster IgG	Jackson ImmunoResearch	107-065-142; RRID: AB_2337458
Cy3-AffiniPure goat anti-rabbit IgG	Jackson ImmunoResearch	111-165-144; RRID: AB_2338006
Goat anti-rabbit-488	Molecular Probes	A31627
Goat anti-rat-546	Molecular Probes	A11081; RRID: AB_141738
Goat anti-VE-Cadherin	R&D Systems	AF1002; RRID: AB_2077789
Hamster anti-mouse TCR β-BV421	BD Pharmingen	562839; RRID: AB_2737830
Mouse anti-human CD11b-PE	eBioscience	12-0118-42; RRID: AB_2043799
Mouse anti-human CD14-FITC	BD Pharmingen	555397; RRID: AB_395798
Mouse anti-human CD31-FITC	BioLegend	303103; RRID: AB_314329
Mouse anti-human HLA-DLR-APC	Thermo Fisher Scientific	17-9956-42; RRID: AB_10670347
Rabbit anti-active CASP3-FITC	BD Pharmingen	550821; RRID: AB_393906
Rabbit anti-Collagen I	Abcam	34710; RRID: AB_731684
Rabbit anti-FITC	AbD Serotec	4510-7604; RRID: AB_620673
Rabbit anti-GAL8	Cloud-Clone	PAA308Mu02
Rabbit anti-GFP	Invitrogen	A21311; RRID: AB_221477
Rabbit anti-hypoxyprobe	Chemicon	HP1-XXX
Rabbit anti-keratin 14	Biolegend	905301; RRID: AB_2565048
Rabbit anti-LYVE1	Angiobio	11-034
Rabbit anti-mouse integrin β1	Abbexa	012440
Rabbit anti-mouse MMP12	LifeSpan Bio	LS-B6312-50; RRID: AB_11043308
Rabbit anti-PDPN	DSHB	8.1.1; RRID: AB_531893
Rabbit anti-PROX1	AngioBio	11-002P; RRID: AB_10013720
Rabbit anti-SMA-Cy3	Sigma-Aldrich	C6198; RRID: AB_476856
Rat anti-activated β1	Pharmingen	553715; RRID: AB_395001

(*Continued on next page*)

Continued

REAGENT or RESOURCE	SOURCE	IDENTIFIER
Rat anti-CD31	BD Pharmingen	550274; RRID: AB_393571
Rat anti-CD34	BD Pharminhen	553731; RRID: AB_395015
Rat anti-CD45	BD Pharmingen	553076; RRID: AB_394606
Rat anti-CD8	eBioscience	14-0808; RRID: AB_2572860
Rat anti-F4/80	AbD Serotec	MCA497; RRID: AB_2098196
Rat anti-human PDPN-APC	Thermo Fisher Scientific	17-9381-41; RRID: AB_10804275
Rat anti-MECA-32	BD Pharmingen	550563; RRID: AB_393754
Rat anti-mouse CD16/C32	BD Pharmingen	553142; RRID: AB_394657
Rat Anti-mouse CD19-BB515	BD Pharmingen	564509; RRID: AB_2738830
Rat Anti-mouse CD4-PE	BD Pharmingen	553049; RRID: AB_394585
Rat anti-mouse CD45-FITC	BioLegend	103108; RRID: AB_312973
Rat Anti-mouse CD90.2-PE	BD Pharmingen	553005; RRID: AB_394544
Rat anti-mouse/human Ki67-BV421	BioLegend	151208; RRID: AB_2629748
Rat anti-VEGFR3	BioLegend	140902; RRID: AB_10680790
VEGFR3-blocking antibody (clone mF431C1)	(Laakkonen et al., 2007)	N/A
Biological Samples		
Breast cancer patient samples	The University Hospitals Gasthuisberg	N/A
Human blood samples	this paper	N/A
Chemicals, Peptides, and Recombinant Proteins		
10 kDa biotin-conjugated dextran	Molecular Probes	D1956
Calcein	Thermo Fisher Scientific	C3099
DNAse I	Sigma-Aldrich	11284932001
DQ Gelatin	Thermo Fisher Scientific	D12054
Evans Blue	Sigma-Aldrich	E2129
Gelatin solution	Sigma-Aldrich	G1393
IgG from rat serum	Sigma-Aldrich	I4131
Methylcellulose 4000 cP	Sigma-Aldrich	M0512
Recombinant GAL8	Novus Biologicals	NBP2-23186
Recombinant murine CCL2	PeproTech	250-10
Tamoxifen	Sigma-Aldrich	T5648
Thiodigalactoside (TDG)	Carbosynth	OG05033
Triton X-100	Sigma-Aldrich	11332481001
WST-1	Sigma-Aldrich	5015944001
Critical Commercial Assays		
Antigen Retrieval solution	DAKO	S1699
CD14 microbeads, human	Miltenyi Biotec	130-050-201
CTX-I ELISA	Hoelzel Diagnostika	KT-72951
Cyanine 3 TSA-Direct Amplification Kit	Perkin Elmer	Nel704A001KT
Cyanine 5 TSA-Direct Amplification Kit	Perkin Elmer	NEL705001KT
Fluorescein TSA-Direct Amplification Kit	Perkin Elmer	Nel701001KT
Fluoromount G	Southern Biotech	0100-01
Interferin	Poluplus Transfection	409-10
LookOut Mycoplasma PCR Kit	Sigma-Aldrich	MP0035
MycoAlert Mycoplasma Detection Kit Plus	Lonza	LT07-705
Pierce Co-Immunoprecipitation Kit	Thermo Fisher Scientific	26149
Pierce ECL Western Blotting Substrate	Thermo Fisher Scientific	32106
PLA Duolink In Situ Red Starter	Sigma-Aldrich	DUO92105
Prolong antifade with DAPI	Molecular Probes	P36935
RIPA Lysis and Extraction Buffer	Thermo Fisher Scietific	89901

(*Continued on next page*)

Continued

REAGENT or RESOURCE	SOURCE	IDENTIFIER
RLT buffer	Qiagen	79216
RNeasy Micro kit	Qiagen	74004
SuperScript III First Strand cDNA Synthesis Kit	Life Technologies	18080051
TaqMan Fast Universal PCR Master Mix	Applied Biosystems	4364103
VEGF-C ELISA kit	MyBioSource	MBS2600109
VEGF-D ELISA kit	MyBioSource	MBS2600462
Viability Dye eFluor-450	eBioscience	65-0863-18
Viability Dye eFluor-506	eBioscience	65-0866-14
Deposited Data		
RNAsequencing data	this paper	GEO: GSE126722
Experimental Models: Cell Lines		
4T1 cell line	ATCC	CRL-2539
Ba/F3-VEGFR3/EpoR cells	(Achen et al., 2000)	N/A
E0771 cell line	CH3 Biosystems	940001
EMT6.5 cell line	(Swierczak et al., 2014)	N/A
Murine BMDMs	this paper	N/A
Experimental Models: Organisms/Strains		
Mouse: constitutive Lgals8$^{-/-}$; C57BL/6J	(Carabelli et al., 2017)	N/A
Mouse: constitutive Pdpn$^{-/-}$; BALB/c	(Mahtab et al., 2008)	N/A
Mouse: Cre-driven line: *Csf1r*.iCre x *Pdpn*$^{lox/lox}$; C57BL/6J	this paper	N/A
Mouse: WT BALB/c	Animalium Gasthuisberg, Leuven, Belgium	N/A
Oligonucleotides		
si*Itgb1*_1	IDT	mm.Ri.Itgb1.13.1
si*Itgb1*_2	IDT	mm.Ri.Itgb1.13.2
si*Itgb1*_3	IDT	mm.Ri.Itgb1.13.3
si*Itgb2*_1	IDT	mm.Ri.Itgb2.13.1
si*Itgb2*_2	IDT	mm.Ri.Itgb2.13.2
si*Itgb2*_3	IDT	mm.Ri.Itgb2.13.3
si*LGALS8*_1	IDT	hs.Ri.LGALS8.13.1
si*LGALS8*_2	IDT	hs.Ri.LGALS8.13.2
si*LGALS8*_3	IDT	hs.Ri.LGALS8.13.3
qRT-PCR primers (Table S1)	IDT	N/A
Recombinant DNA		
pLKO.3-GAL8-HA plasmid	this paper	N/A
Software and Algorithms		
CellSense Dimension software	Olympus	N/A
GraphPad Prism software	GraphPad	7.0
ImageQuant software	GE Health Care	TL8.1
Imaris 9.2 software	BITPLANE	N/A
Nikon NIS-Elements software	Nikon	N/A
Other		
6.5 mm Transwell with 8.0 μm Pore Polyester Membrane Insert	Corning	3464
Collagen type I	BD Biosciences	354249
Collagenase I	Thermo Fisher Scientific	17100017
Dispase	Gibco	17105-041
Dulbecco's Modified Eagle Medium (DMEM)	Gibco	41965120
Dulbecco's phosphate-buffered saline (DPBS)	Thermo Fisher Scientific	14190144

(*Continued on next page*)

Continued

REAGENT or RESOURCE	SOURCE	IDENTIFIER
EGM-2 medium	Lonza	CC-3202
FBS (Fetal Bovine Serum)	Biochrom BmgH	S0115
Matrigel	Corning	354230
OCT compound	Leica	20108926
ProLong Gold Antifade Mounting Solution	Thermo Fisher Scientific	P36930
Red blood cell lysing buffer Hybri-Max	Sigma-Aldrich	R7757
RPMI-1640 medium	Gibco	11875093
Trypsin-EDTA (0,25%)	Thermo Fisher Scientific	25200056
Trypsin-EDTA (0.25%)	Thermo Fisher Scientifi	25200056

LEAD CONTACT AND MATERIALS AVAILABILITY

Further information and requests for resources and reagents should be directed to and will be fulfilled by the Lead Contact, Massimiliano Mazzone (massimiliano.mazzone@kuleuven.vib.be).

This study did not generate new unique reagents.

EXPERIMENTAL MODEL AND SUBJECT DETAILS

Animals

Constitutive *Pdpn*-deficient mice in a 129S/v X Swiss (50/50) background (Mahtab et al., 2008; Uhrin et al., 2010) (a kind gift of Dr. Dontscho Kerjaschki from the University of Vienna, Austria) were backcrossed for 8 generations into a BALB/c background.

Conditional *Pdpn* knockout mice were generated in a C57BL/6J background using a targeted ES cell line from KOMP/EUCOMM (EPD0636_3_B09). Positive clones were confirmed by Southern Blot. The NEO cassette was deleted *in vivo* by using FLP-mediated recombination. The final transgenic line carries 2 LoxP- sites within the exon 1 in each *Pdpn* allele. Finally, we generated *Csf1r*.iCre x $Pdpn^{lox/lox}$ mice in a C57BL/6J background by intercrossing $Pdpn^{lox/lox}$ mice with the tamoxifen-inducible, macrophage specific *Csf1r*.iCre deleter mouse line. *Csf1r*.iCre x $Pdpn^{wt/wt}$ littermates were used as controls. Acute deletion of *Pdpn* in macrophages was obtained by intraperitoneal injections of Tamoxifen (Sigma-Aldrich, T5648) (1mg/mouse/day) for 5 consecutive days prior to orthotopic implantation of E0771 cancer cells. Control mice were treated with Tamoxifen according to the same protocol.

Constitutive *Lgals8* knockout mice in a C57BL/6J background (Carabelli et al., 2017) were a gift of Dr. María Virginia Tribulatti from Universidad Nacional de San Martín, Buenos Aires, Argentina.

All mice used for tumor experiments were females between 8 and 15 weeks old. Housing and all experimental animal procedures were approved by the Institutional Animal Care and Research Advisory Committee of the KU Leuven.

Cell Lines

4T1 and E0771 medullary breast adenocarcinoma cell lines were obtained from the American Type Culture Collection (ATCC) and CH3 Biosystems, respectively. The 4T1 cells were cultured in DMEM (Gibco) supplemented with 10% Fetal Bovine Serum (Gibco), 100 units/ml penicillin and 100 μg/ml streptomycin. The E0771 cells were cultured in RPMI (Gibco) supplemented with 10% Fetal Bovine Serum (Gibco), 100 units/ml penicillin and 100 μg/ml streptomycin. EMT6.5 cells were a kind gift from Dr. Robin L. Anderson (Peter MacCallum Cancer Centre, Melbourne, Australia). They were cultured in MEM alpha (Lonza) supplemented with 10% Fetal Bovine Serum (Gibco), 100 units/ml penicillin and 100 μg/ml streptomycin. HMVECs (Human microvascular endothelial cells) were obtained from Lonza and cultured in EBM-2 medium (Lonza) supplemented with hEGF, hydrocortisone, gentamicin, amphotericin, FBS (5%), VEGF, hFGF, hR3-IGF-1, and ascorbic acid. All cells were maintained in a humidified incubator in 5% CO_2 at 37°C. 0.1% pork gelatin (Sigma-Aldrich) was used to stimulate the adhesion HMVECs to the flask bottom. All cancer cell lines underwent mycoplasma testing before their use. Negative mycoplasma contamination status was verified using LookOut Mycoplasma PCR Kit (Sigma-Aldrich) and MycoAlert Mycoplasma Detection Kit plus Assay Control (Lonza).

Cell Isolation and Culture

Murine Bone Marrow-Derived Macrophages (BMDMs)

Macrophages were derived from bone marrow precursors as described before (Casazza et al., 2013). Briefly, bone marrow cells (1×10^7 cells) were cultured in a volume of 6 ml in a 10 cm Petri dish (non-tissue culture treated, bacterial grade) in DMEM supplemented with 20% FBS and 30% L929-conditioned medium as a source of M-CSF. After 3 days in culture, the medium was supplemented with additional 3 ml of the differentiation medium. At day 7, BMDMs were harvested with ice cold Ca^{2+}- and Mg^{2+}-free PBS. The cells obtained were uniformly macrophages as assessed by FACS, using the myeloid cell-specific marker CD11b and the pan-macrophage-specific marker F4/80.

Murine Tumor-Associated Macrophages

4T1 tumor-bearing mice were sacrificed by cervical dislocation and tumors were collected in cold PBS. Tumors were then minced in RPMI medium containing 0,1% collagenase type I and 0,2% dispase type I and incubated in the same solution for 30 minutes at 37°C. The digested tissue was filtered using a 70 μm strainer and cells were centrifuged for 5 minutes at 1000 rpm. Red blood cell lysis was applied by using a Hybri-Max solution (Sigma-Aldrich). Cells were re-suspended in FACS buffer and incubated for 15 minutes with Mouse BD Fc BlockTM purified anti-mouse CD16/CD32 antibody (BD Pharmingen) and stained with the following antibodies for 30 minutes at 4°C, protected from light: viability dye (eF450 or eF506), anti-CD11b (M1/70), anti-F4/80 (BM8), anti-PDPN (8.1.1., BioLegend). The antibodies were purchased from Thermo Fischer Scientific (eBioscience), unless specified differently. Cells were then washed and re-suspended in cold FACS buffer before flow sorting by FACS Aria (BD Biosciences). FMO (Fluorescence Minus One) controls were utilized in order to ensure proper gating of positive populations. Isolated TAMs (PoEMs, non-PoEMs, WT pool or KO pool) were cultured in DMEM (Gibco) supplemented with 10% Fetal Bovine Serum (Gibco), 100 units/ml penicillin and 100 μg/ml streptomycin and maintained in a humidified incubator in 5% CO_2 at 37°C.

Human Tumor-Associated Macrophages

Fresh human breast cancer specimens were obtained from the University Hospital Gasthuisberg (Leuven, Belgium) and cut into small pieces and digested in PBS with Liberase DL, Liberase TL (Roche) and DNase I (Sigma-Aldrich) in serum-free PBS. The digestion was performed using a MACS dissociator, following the manufactures' instructions (Miltenyi Biotec). After digestion, tumor samples were re-suspended in PBS 2% FBS, 2mM EDTA and filtered through a 70 μm strainer. Red blood cell lysis was performed prior to the Fc blocking (eBioscience, 14-9161-71), followed by staining with the following FACS antibodies: anti-CD11b (eBioscience, ICRF44), anti-CD14 (BD Pharmingen, M5E2), anti-HLA-DR (eBioscience, LN3), anti-PDPN (eBioscience, NZ-1.3). Cells were then washed and resuspended in cold FACS buffer before flow sorting by FACS Aria (BD Biosciences). FMO (Fluorescence Minus One) controls were utilized in order to ensure proper gating of positive populations. Isolated TAMs were used in migration assays and cultured in DMEM (Gibco) supplemented with 10% Fetal Bovine Serum (Gibco), 100 units/ml penicillin and 100 μg/ml streptomycin and maintained in a humidified incubator in 5% CO_2 at 37°C. The clinical protocol was approved by the Ethical Committee of the University Hospitals Gasthuisberg (Leuven, Belgium), and all subjects consented prior to study participation.

Human Monocyte-Derived Macrophages

Human monocytes were obtained from healthy blood donor buffy coats under an institutional review board-approved protocol and isolated with CD14-conjugated MicroBeads (Miltenyi Biotec) as described previously (Palmieri et al., 2015).

Human Umbilical Endothelial Cells

HUVECs were freshly isolated from umbilical cords obtained from multiple donors (with approval from the Ethics Committee Research UZ/KU Leuven and informed consent obtained from all subjects) as previously described (Schoors et al., 2015) and regularly tested for mycoplasma. They were maintained in M199 medium (Invitrogen) supplemented with 20% FBS, 2 mM glutamine, 100 units/ml penicillin, 100 μg/ml streptomycin, 0.15% heparin and 20 μg/ml ECGS (Sigma-Aldrich). 0.1% pork gelatin (Sigma-Aldrich) was used to stimulate the adhesion HUVECs to the flask bottom.

Breast Cancer Patients

Paraffin-embedded tumor samples from 19 patients with bilateral breast carcinomas were analyzed histologically for the presence of PoEMs in the lymphatic niche. The clinical protocol was approved by the Ethical Committee of the University Hospitals Gasthuisberg (Leuven, Belgium), and all subjects consented prior to study participation. Detailed tumors' characteristics are listed in Table S2.

METHOD DETAILS

Assessment of LEC Identity, Proliferation and Apoptosis

5 x 10^4 LECs were cultured in EGM-2 medium in 6-well plates alone or together with different populations of sorted BMDMs (in ratio 1:1) for 24 h. Then, LECs were detached with Trypsin, washed in PBS and re-suspended in FACS buffer (PBS containing 2% FBS and 2 mM EDTA). Cells were stained with the following antibodies: Ki67 (Biolegend, 11F6), anti-active CASP3 (BD Pharmingen, C92-605), anti-PDPN (eBioscience, NZ-1.3), anti-CD31 (eBioscience WM59). Cells were then washed and resuspended in cold FACS buffer before FACS analysis with a FACS Verse (BD Biosciences). FMO (Fluorescence Minus One) controls were utilized in order to ensure proper gating of positive populations.

Assessment of Intercellular GAPs in LEC Monolayers

5 x 10^4 LECs (HMVECs) were seeded on gelatin-coated cover slips in 24-well plates in EGM-2 medium. The medium was changed every second day. On day 5, BMDMs derived from WT or *Pdpn* KO BM cells were sorted into 4 populations (PoEMs, non-PoEMs, WT pool, *Pdpn* KO pool), incubated for 20 minutes on ice with an anti-β1 blocking antibody (clone HMβ1-1, Biolegend) or with isotype control and seeded on top of LECs (1 x 10^5 sorted BMDMs per well). 16 h later, the coverslips were washed once with PBS and fixed in 4% PFA for 30 minutes. The cells were then blocked in PBS with 1% BSA, 0,3% TritonX 100 for 1 h. Samples were next incubated overnight at 4°C with a goat anti-VE-CADHERIN antibody (R&D Systems) and subsequently incubated with rabbit anti-goat-Cy3 secondary antibody (Jackson). The samples were then washed with PBS and mounted on glass slides with Prolong Gold antifade mounting medium with DAPI (Thermo Fisher).

Ba/F3 Viability Assay

Immortalized cancer-associated fibroblasts (CAFs) (a kind gift from Dr. Sarah-Maria Fendt from VIB Center for Cancer Biology, Leuven, Belgium) from human breast tumors were starved for 48 h in DMEM 1% P/S. F4/80^{+} CD11b^{+} TAMs were sorted from 4T1 tumors bore by WT or *Pdpn* KO bone marrow chimeras and cultured for 48 in medium derived from the starved CAFs (in a ratio TAM medium/CAF medium: 5/3). The CAF medium constituted the source of pre-mature VEGFC (see Figure S3Q). Next, Ba/F3 cells expressing the VEGFR-3/EpoR chimera (a kind gift from Prof. Kari Alitalo from the University of Helsinki, Finland) were cultured in the TAM/CAF media or separately in either of those for 72h in 96 well plates (at 15.000 cells/well). The survival of Ba/F3 cells was assessed using WST-1 survival assay according to the manufacturer's protocol (Sigma-Aldrich, 5015944001) (incubation time – 1h).

BMDM-LEC Adhesion Assay

5 x10^{3} HMVECs were seeded in EGM-2 medium in a 96-multiwell plate, previously coated with Matrigel. 16 hours later, 5 x10^{3} Calcein-labelled BMDMs were added on top in EGM-2 medium. 6 hours later, the wells were washed briefly with PBS and fixed in 4% PFA. The adhesion of BMDMs to HMVEC capillaries was visualized using a Leica DMI6000 microscope.

Bone Marrow Transplantation

In order to generate *Pdpn* bone marrow chimeras (BM), 5-6 weeks old Balb/c recipient mice were irradiated with 7,5 Gy. Subsequently, 5 x 10^{6} bone marrow cells from donor mice of the appropriate genotype (*Pdpn* WT or *Pdpn* KO) were injected intravenously via the tail vein. Tumor experiments were initiated 6 weeks after BM reconstitution.

In order to generate *Csf1r*;*Pdpn* BM chimeras, 5-6 weeks old C57BL/6J recipient mice (either *Lgals8* WT or *Lgals8* KO) were irradiated with 9,2 Gy. Subsequently, 5 x 10^{6} bone marrow cells from donor mice of the appropriate genotype (*Csf1r*;*Pdpn*$^{wt/wt}$ or *Csf1r*;*Pdpn*$^{lox/lox}$) were injected intravenously via the tail vein. 5 weeks after BM reconstitution, *Pdpn* in macrophages was deleted by intraperitoneal injections of Tamoxifen (Sigma-Aldrich, T5648) (1mg/mouse/day) for 5 consecutive days. Tumor experiments were initiated 3 days after termination of the Tamoxifen treatment.

Collagen I Degradation by 4T1 TAMs Ex Vivo

Different sorted 4T1 TAM populations (PoEMs, non-PoEMs, WT pool, *Pdpn* KO pool) were seeded in 96 well plate (1 x 10^{4} TAMs per well) and cultured for 72 h in DMEM complete. Culture supernatants were collected and the presence of CTX-1 (type I collagen cross-linked C-telopeptide) was detected by ELISA kit (Hoelzel Diagnostika), according to the manufacturer's protocol.

Corneal Cauterization Assay

The corneal cauterization experiment was performed as previously described (García-Caballero et al., 2017). Briefly, 8-week-old female *Pdpn* WT and KO chimeras were anesthetized with intraperitoneal injection of ketamine hydrochloride (100 mg/kg) and xylazine (10 mg/kg). Then, a local anaesthetic (Unicaïne 0,4%; Thea Pharma) was applied in the eye and the central part of the cornea was thermally cauterized using an ophthalmic cautery (Optemp II V; Alcon Surgical, Fort Worth, TX). Mice were sacrificed after 9 days post-injury, the eyes were removed and corneas harvested. Whole-mounted corneas were fixed in 70% ethanol for 1 hour at room temperature and blocked with 3% BSA in PBS for 1 hour. Corneas were incubated overnight with rabbit anti-mouse Lyve1 and rat anti-mouse CD31 antibodies and subsequently incubated with AlexaFluor 488-conjugated goat anti-rabbit antibody and AlexaFluor 546-conjugated goat anti-rat secondary antibodies (Molecular Probes, Merelbeke) for 2 hours. Corneas were flat-mounted on a microscope slide with Prolong Gold antifade mounting medium (Thermo Fisher) and imaged using a Leica DMI6000 microscope (Leica Microsystems).

FACS Analysis and Flow Sorting of Human TAMs

Human breast cancer specimens were cut into small pieces and digested in PBS with Liberase DL, Liberase TL (Roche) and DNase I (Sigma-Aldrich) in serum-free PBS. The digestion was performed using a MACS dissociator, following the manufactures' instructions (Miltenyi Biotec). After digestion, tumor samples were re-suspended in PBS 2% FBS, 2mM EDTA and filtered through a 70 μm strainer. Red blood cell lysis was performed prior to the Fc blocking (eBioscience, 14-9161-71), followed by staining with the following FACS antibodies: anti-CD11b (eBioscience, ICRF44), anti-CD14 (BD Pharmingen, M5E2), anti-HLA-DR (eBioscience, LN3), anti-PDPN (eBioscience, NZ-1.3). Cells were then washed and resuspended in cold FACS buffer before FACS analysis or flow sorting by a FACS Verse or FACS Aria (BD Biosciences), respectively. FMO (Fluorescence Minus One) controls were utilized in order to ensure proper gating of positive populations.

FACS Analysis and Flow Sorting of Murine Tissue- and Tumor-Infiltrating Leukocytes

4T1 tumor-bearing mice were sacrificed by cervical dislocation and tumors and draining lymph nodes were collected in cold PBS. Lymph nodes were dissociated mechanically by pressing with a syringe plunger and collected in FACS buffer (PBS containing 2% FBS and 2 mM EDTA). Tumors were minced in RPMI medium containing 0,1% collagenase type I and 0,2% dispase type I and incubated in the same solution for 30 minutes at 37°C. The digested tissue was filtered using a 70 μm strainer and cells were centrifuged for 5 minutes at 1000 rpm. Red blood cell lysis was applied by using a Hybri-Max solution (Sigma-Aldrich). Cells were re-suspended in FACS buffer and incubated for 15 minutes with Mouse BD Fc BlockTM purified anti-mouse CD16/CD32 antibody (BD Pharmingen) and stained with the following antibodies for 30 minutes at 4°C, protected from light: viability dye (eF450 or eF506), anti-CD45

(30-F11), anti-CD11b (M1/70), anti-F4/80 (BM8), anti-TCRβ (H57-597), anti-CD4 (RM4-5), anti-CD8 (53-6.7), anti-MHCII (M5/114.15-12) , anti-CD11c (N418), anti-CD19 (1D3), anti-NKp46 (29A1.4), anti-CD115 (AFS98), anti- Ly6G (14A8), anti-CD204 (REA148, Mylteni Biotec), anti-CD90.2 (53-2.1, BD Pharmingen), anti EpCAM (G8.8) and anti-PDPN (8.1.1., BioLegend). The antibodies were purchased from Thermo Fischer Scientific (eBioscience), unless specified differently. Cells were then washed and re-suspended in cold FACS buffer before FACS analysis or flow sorting by a FACS Verse or FACS Aria (BD Biosciences), respectively. FMO (Fluorescence Minus One) controls were utilized in order to ensure proper gating of positive populations.

Gelatin Degradation by 4T1 TAMs Ex Vivo

Different sorted 4T1 TAM populations (PoEMs, non-PoEMs, WT pool, *Pdpn* KO pool) were seeded in fluorescein gelatin-coated wells (Life Technologies) of a 96-well plate (1 x 10^4 TAMs per well) and cultured for 72 h in DMEM complete. Culture supernatants were collected and the presence of green fluorescence (indicating proteolytic digestion of DQ fluorescein-labelled gelatin) was assessed spectrophotometrically at 485 nm.

Gene Silencing *In Vitro*

Silencing of *LGALS8* in LECs (HMVECs) was achieved by in vitro siRNA transfection with INTERFERin (Polyplus), following the manufacter's instructions. Briefly, LECs were seeded in 24-well plates (0,5 x 10^6 LECs/well) and transfected with 30 nM of total siRNA from IDT. The following oligos were used as pooled or separately: (A) hs.Ri.LGALS8.13.1, (B) hs.Ri.LGALS8.13.2 and (C) hs.Ri.LGALS8.13.3. Control LECs were transfected with scrambled siRNA sequences. Silencing efficiency was assessed by qRT-PCR.

Histology and Immunostainings

For serial 7 μm thick tumor, lung or lymph node sections, tissue samples were fixed in 2% PFA overnight at 4°C, dehydrated and embedded in paraffin. Tumor samples for thick sections (80 μm thick) were fixed overnight in 4% PFA and cryopreserved in 15% sucrose for 10 h and then in 30% sucrose overnight. The samples were then snap-frozen in OCT compound (Tissue-Tek). Tumor samples for vibratome sections (E0771 tumors from R26.mTmG;*Csf1r*.Cre mice and 4T1-GFP tumors from *Pdpn* BM chimeras) were fixed overnight in 4% PFA and washed 3 x 30 minutes in PBS. Subsequently, the sections were embedded in 3% low melting point agarose and sectioned on vibratome into 150 μm thick sections. The sections were then blocked and permeabilized in TNBT (0.1 M Tris pH 7.4; NaCl 150 mM; 0.5% blocking reagent from Perkin Elmer, 0.5% Triton X-100) for 4 h at room temperature. Human breast cancer samples were obtained as 7 μm thick paraffin-embedded slides. Paraffin slides were first rehydrated to further proceed with antigen retrieval in citrate solution (DAKO) at 100°C for 20 minutes. Thick cryo-sections were thawed and fixed in 100% methanol. If necessary, 0.3% hydrogen peroxide was added to methanol in order to block the activity of endogenous peroxidases. The sections were blocked with the appropriate serum (DAKO) and incubated overnight with the following primary antibodies: rabbit anti-PDPN (DSHB, 8.1.1), rabbit anti-LYVE1 (Angiobio, 11-034), rat anti-VEGFR3 (Biolegend, 140902), rabbit anti-PROX1 (AngioBio, 11-002P), rat anti-CD34 (BD Pharminhen, 553731), rat anti-CD31 (BD Pharmingen 550274), rabbit anti-FITC (AbD Serotec, 4510-7604), rabbit anti-GFP (Invitrogen, A21311), rat anti-F4/80 (AbD Serotec, MCA497), rabbit anti-GAL8 (Cloud-Clone, PAA308Mu02), rat anti-activated β1 (BD Pharmingen, 553715), rabbit anti-SMA-Cy3 (Sigma-Aldrich, C6198), rabbit anti-hypoxyprobe (Hypoxyprobe kit, Chemicon), rabbit anti-keratin 14 (Biolegend, 905301), rat anti-CD8 (eBioscience 14-0808), rat anti-CD45 (BD Pharmingen, 553076), rat anti-MECA-32 (BD Pharmingen, 550563), rabbit anti-mouse MMP12 (LifeSpan Bio, LS-B6312-50), rabbit anti-Collagen I (Abcam, 34710), anti-human PDPN (eBioscience, 14-9381-82), anti-human CD68 (Dako, M0876), anti-human CD45 (Sino Biological, 100342-R145), anti-human GAL8 (GTX, 117687), anti-human MECA-32 (GTX, 54474). Next, appropriate secondary antibodies were applied: Alexa 488, 647 or 568 conjugated secondary antibodies (Molecular Probes) in concentration 1:200 or biotin-labeled antibodies (Jackson Immunoresearch) in concentration 1:300. After biotin-labelled antibodies, TSA fluoresceine, TSA Cyanine 3 or Cyanine 5 system amplification kits (Perkin Elmer, Life Sciences) were utilized according to the manufacturer's instructions. Hoest solution (1/1000) was utilized in order to visualize nuclei. Mounting of slides was done with ProLong Gold mounting medium without DAPI (Invitrogen). Imaging and microscopic analysis was performed with an Olympus BX41 microscope and CellSense imaging software. For morphological analysis of TAMs interacting with lymphatic vessels and/or cancer cells, confocal images of thick cryo- or vibratome sections were acquired with a Zeiss Axioplan microscope with KS300 image analysis software. Z-stacks were assembled to maximum intensity projections.

Immunofluorescence in BMDMs

Mature BMDMs were seeded on cover slips in 24-well plates (200.000 cells/well) and treated accordingly to an experimental design. Prior to incubation with recombinant GAL8 (Novus Biologicals), cells were washed with PBS and incubated for 12 h in DMEM without FBS. In all experiments, treatment with GAL8 (or PBS) lasted for 40 minutes in FBS-deprived DMEM (1% P/S). Subsequently, the cells were washed once with PBS and fixed in 4% PFA for 30 minutes. The cells were then blocked and permaebilized in PBS with 1% BSA, 0,3% TritonX 100 for 1 h. Samples were next incubated overnight at 4°C with primary antibodies: rabbit anti-GAL8 (BioConnect) or rat anti-activated B1 (BD Pharmingen) and subsequently incubated with appropriate secondary antibodies: goat anti-rabbit-Cy3 and AlexaFluor 488-conjugated goat anti-rat. The samples were then washed with PBS and mounted on glass slides with Prolong Gold antifade mounting medium with DAPI (Thermo Fisher).

Immunofluorescence in Sorted TAMs

$CD11b^+$, $F4/80^+$, $PDPN^+$ or $PDPN^-$ cells sorted from 4T1 tumors bore by WT or *Pdpn* KO chimeras were seeded on cover slips in 24-well plates (30.000 cells/well) and grown in DMEM complete for 72 h. The cells were washed once with PBS and cover slips were decellularized with a pre-warmed extraction buffer (20 mM NH4OH, 0.5% Triton X-100 in PBS) for 5 minutes. The slips were washed twice with PBS and fixed in 4% PFA for 30 minutes, followed by another PBS wash. Samples were next incubated overnight at 4°C with an anti-Collagen 1 antibody (Abcam) and subsequently incubated with a secondary antibody: goat anti-rabbit-Cy3. The samples were then washed with PBS and mounted on glass slides with Prolong Gold antifade mounting medium with DAPI (Thermo Fisher).

Injection of 4T1 Cancer Cells into Lymph Nodes

2×10^4 4T1 cancer cells were directly deposited in the inguinal lymph nodes of WT→WT or *Pdpn* KO→WT chimeras by means of intralymphatic microinfusion, as described previously (Braun et al., 2011). After 30 days, mice were sacrificed and lung metastatic nodules were contrasted upon intratracheal injection of 15% India ink solution. Superficial metastatic nodules were assessed under a stereomicroscope.

Intratumoral Thiodigalactoside (TDG) Treatment

4 days after 4T1 tumor cells implantation, mice received 120 mg/kg TDG (Carbosynth) or vehicle (PBS) injected intratumorally. The treatment was repeated 3 times per week, until the experiment was terminated.

Intratumoral VEGFR3-Blocking Antibody Treatment

4 days after 4T1 tumor cells implantation, mice received 40 μg/g VEGFR3-blocking antibody (clone mF431C1), which was a kind gift from Dr. Sudhakar Chintharlapalli of Eli Lilly and Company, or IgG control injected intratumorally. The treatment was repeated 2 times per week, until the experiment was terminated.

LEC Capillary-like Structure Formation Assay

5×10^3 HMVECs were seeded together with 5×10^3 BMDMs in EGM-2 medium in a 96-multiwell plate, previously coated with Matrigel. 6 hours later, the wells were washed briefly with PBS and fixed in 4% PFA. The capillary-like structure formation by LECs was visualized using a Leica DMI6000 microscope.

Lgals8 Overexpression in LECs

For the overexpression of murine *Lgals8* gene in LECs (HMVECs), the corresponding ORF (NM_001199043.1) was sub-cloned in a lentiviral vector backbone in order to obtain the pLKO.3-GAL8-HA expression cassette. Amplified viral particles were purified and titrated, and subsequently used for LEC infection.

Lung Colonization Assay

$0{,}5 \times 10^6$ 4T1 cancer cells were injected in the tail vein of WT→WT or *Pdpn* KO→WT chimeras. After 12 days, mice were sacrificed and lung metastatic nodules were contrasted upon intratracheal injection of 15% India ink solution. Superficial metastatic nodules were assessed under a stereomicroscope.

Lymphangiography

4T1 tumor-bearing mice (at day 22 of tumor growth) were anesthetized and injected intratumorally with 6 mg of Evans Blue in 100 μL of sterile PBS per 20 g of mouse body weight. 20 minutes later, mice were sacrificed by cervical dislocation and tumor-draining lymph nodes were harvested, washed in PBS and digested in 200 μl of formamide at 60°C for 48 h. The amount of extravasated Evans Blue dye was quantified with a spectrophotometer at 630 nm.

Macrophage Migration Assays

In the macrophage migration assays, 1×10^5 murine BMDMs, 1×10^5 $CD11b^+$ $F4/80^+$ TAMs (sorted from 4T1 tumors), 1×10^5 $CD11b^+$, $CD14^+$ human monocyte-derived-macrophages or 1×2^4 $CD11b^+$, $CD14^+$, $HLA\text{-}DR^+$ TAMs (sorted from human breast tumor specimens) were labelled with Calcein (Molecular Probes) and seeded on 8 μm polycarbonate membrane (Transwell; Costar). For some assays, the BMDMs were incubated for 20 minutes on ice with an anti-β1 blocking antibody (clone HMβ1-1, Biolegend) or with isotype control prior to the migration. The bottom chambers contained DMEM with specific chemoattractants, inhibitors or controls (specified in each figure). When indicated, HMVECs (LECs) were seeded in the bottom chambers 16 h prior to the macrophage migration. After 4h incubation, the cells were removed from the top of each membrane with a cotton stick and migrated cells were fixed in 4% PFA, washed in PBS and mounted on glass slides with ProLong Gold mounting medium with DAPI. Alternatively, cells on the top (non-migrated) or the bottom (migrated) side of a Transwell were stained for PDPN and DAPI, using a standard immunofluorescence protocol. Images were acquired with Olympus BX41 microscope and CellSense imaging software.

Metastatic Tumor Models

1 x 10^6 4T1 or E0771 breast adenocarcinoma cells or 1 x 10^5 EMT6.5 cells were injected orthotopically to the right mammary fat pad of the second nipple in a volume of 50 μl PBS. For specific assays, lymphadenectomy of inguinal tumor-draining lymph nodes was performed 7 days prior to 4T1 cell inoculation in the mammary pads. Tumor volumes were measured three times a week with a caliper and calculated using the formula: V = π x [d2 x D] / 6, where d is the minor tumor axis and D is the major tumor axis. At the end stage, tumor weight was registered and samples were collected for histological examination or FACS/sorter analysis. Lung metastatic nodules were contrasted after intratracheal injection of 15% India ink solution. Superficial metastatic nodules were assessed under a stereomicroscope. Alternatively, lung metastasis was assessed by hematoxylin-eosin staining on paraffin sections.

PDPN-Integrin β1 Co-immunoprecipitation

Rat IgG (5 μg, Sigma-Aldrich) and anti-Integrin β1 (5 μg, clone 9EG7, BD Pharmigen) were immobilized onto AminoLink Plus coupling resin (Pierce) by sodium cyanoborohydride according to the manufacturer's instructions. BMDMs were lysed with IP lysis/wash buffer (25 mM Tris, 150 mM NaCl, 1 mM EDTA, 1% NP-40, 5% glycerol; pH 7.4) supplemented with protease inhibitor cocktails (Roche). After centrifugation (10 minutes, 13,000 rpm) supernatants (1,5 mg protein lysates) were pre-cleared by incubation for 1 h with Pierce control agarose resin at 4°C. The clarified samples were incubated with the antibody-conjugated agarose resins overnight at 4°C. Immunoprecipitates were washed three times with IP lysis/wash buffer and once with conditioning buffer provided in the kit (Pierce). The bound proteins were eluted with an elution buffer and analyzed alongside with input by Western blot, using anti-integrin β1 (R&D, AF2405) and anti-PDPN (DSHB, 8.1.1) antibodies. Signal was visualized by Enhanced Chemiluminescent Reagents (ECL, Invitrogen), according to the manufacturer's instructions and acquired by a LAS 4000 CCD camera with ImageQuant software (GE Healthcare).

Perilymphatic TAMs

The adhesion of TAMs to lymphatic vessel walls was assessed upon performing a triple staining on paraffin-embedded tumor sections: F4/80, Pdpn and VEGFR3, in order to ensure that only lymphatic vessels ($Pdpn^+$, $VEGFR3^+$) are taken into account. The numbers of $F4/80^+$ macrophages that were in direct touch with lymphatic endothelium were normalized per total TAM number. This ratio was then divided for the overall lymphatic area in a field. For each tumor, the average of 5 independent fields was quantified.

Proximity Ligation Assay (PLA)

WT or *Pdpn* KO BMDMs were seeded on cover slips in 24-well plates (2 x 10^5 cells/well) and incubated overnight without FBS. The following day, the cells were treated with GAL8 (Novus Biologicals) (or PBS) for 40 minutes in FBS-deprived DMEM (1% P/S). For the PLA, the Duolink In Situ Red Starter Kit Goat/Rabbit (Sigma-Aldrich) was utilized according to the manufacturer's protocol. The following primary antibodies were used: goat anti-mouse PDPN (R&D Systems, AF3244), rabbit anti-mouse integrin β1 (Abbexa, 012440). Interactions between the proteins was visualized using Olympus BX41 microscope and CellSense imaging software.

qRT-PCR

Cells or tissue supernatants were washed in PBS, collected in RLT buffer (Qiagen) and stored at -80°C. RNA was extracted with the RNeasy Micro kit (Qiagen) according to the manufacturer's instructions. Reverse transcription to cDNA was performed with the SuperScript III First Strand cDNA Synthesis Kit (Life Technologies) according to manufacturer's protocol. Pre-designed assays were purchased from IDT. cDNA, primer/probe mix and TaqMan Fast Universal PCR Master Mix were prepared in a volume of 10 μl according to manufacturer's instructions (Applied Biosystems). Samples were loaded into an optical 96-well Fast Thermal Cycling plate (Applied Biosystems) and qRT-PCR reactions were performed using an ABI Prism 7500 Fast Real-Time PCR System (Applied Biosystems).

RNA Sequencing

RNA concentration and purity from freshly sorted TAMs were determined spectrophotometrically using the Nanodrop ND-1000 (Nanodrop Technologies) and RNA integrity was assessed using a Bioanalyzer 2100 (Agilent). Per sample, an amount of 100 ng of total RNA was used as input. Subsequently, 5 ng of purified cDNA was sheared to 300 bp using the Covaris M220. From the sheared material, sequencing libraries were prepared with the NEBNext Ultra DNA Library Prep Kit for Illumina (version 6.0 -2/18), according to the manufacturer's protocol including a size selection to 250 bp insert size. Sequence-libraries of each sample were finally equimolarly pooled and sequenced on 1 NextSeq500 v2 flow-cell at 1x75 bp (76-6-0-0).

Spheroid LEC Sprouting Assay

In order to generate hybrid multicellular microspheres, LECs and different populations of sorted BMDMs were mixed in a 3:1 ratio and incubated for 24 h in hanging drops in EGM-2 medium containing 20% methylcellulose 4000 cP (Sigma-Aldrich). Spheroids were then embedded in Collagen I gel as previously described (Heiss et al., 2015) and maintained at 37°C for 24 hours to induce sprouting. Cultures were then fixed with 4% PFA at room temperature and phase contrast images were taken with a Leica DMI6000 microscope. Analysis of the number of sprouts per spheroid and the total sprout length (cumulative length of primary sprouts and branches per spheroid) was done on images using the CellSense imaging software.

Three-Dimensional Reconstructions of TAM-Lymphatic Vessel-Cancer Cell Triads

Stained vibratome sections from 4T1-GFP$^+$ tumors were imaged with a Nikon A1 Confocal microscope using Z-stacks of the calculated optimal travel range of 1.1μm and to an average depth of 70μm. Automatic Z-stack intensity equalization was performed with the Nikon NIS software followed by further image analysis using Imaris 9.2 software. In brief, lymphatic vessels were automatically 3D-reconstructed in order to measure the total LYVE1 surface area of these vessels. Afterwards, the triads of macrophages and tumor cells co-interacting with these recognized vessel structures were counted manually and normalized to the previously measured LYVE1 surface area. As a final step, also macrophages and cancer cells were 3D-reconstructed in order to generate the representative images.

Transendothelial Invasion Assay

5 x 10^4 LECs (HMVECs) were seeded on 8 μm polycarbonate membrane (Transwell; Costar) in EGM-2 medium. 72 h later, BMDMs derived from WT or *Pdpn* KO BM cells were sorted into 4 populations (PoEMs, non-PoEMs, WT pool, *Pdpn* KO pool), incubated for 20 minutes on ice with an anti-β1 blocking antibody (clone HMβ1-1, Biolegend) or with isotype control and seeded on top of LECs (1 x 10^5 sorted BMDMs per membrane). 16 h later, Transwells were placed in wells containing fresh DMEM with 10% FBS. 4T1 cancer cells were labelled with Calcein and seeded on top of the LEC-BMDM co-cultures (1 x 10^5 4T1 cells in 100 μl DMEM 10% FBS per membrane). After 4h incubation, the cells were removed from the top of each membrane with a cotton stick and migrated cells were fixed in 4% PFA, washed in PBS and mounted on glass slides with ProLong Gold mounting medium with DAPI. Images were acquired with Olympus BX41 microscope and CellSense imaging software.

Tumor Hypoxia Assessment

Tumor hypoxia was detected 1h after intraperitoneal injection of 60 mg/kg pimonidazole hydrochloride into 4T1 or E0771 tumor-bearing mice. Mice were sacrificed and tumors harvested and fixed in 2% PFA overnight. To detect the formation of pimonidazole adducts, the sections were immunostained with an anti-hypoxyprobe-1 monoclonal antibody (Hypoxyprobe kit, Chemicon), following the manufacturer's instructions.

VEGFC and VEGFD ELISA

Different sorted 4T1 TAM populations (PoEMs, non-PoEMs, WT pool, *Pdpn* KO pool) were seeded in gelatin-coated wells of a 96-well plate (1 x 10^4 TAMs per well) and cultured for 72 h in DMEM complete. Culture supernatants were collected, cells were gently harvested in PBS with a pipet tip and lysed in RIPA buffer (Thermo Scientific), and the extracellular matrix (gelatin) proteins were directly lysed in RIPA (Thermo Scientific), as described previously (Du et al., 2008). The presence of VEGFC or VEGFD in the abovementioned fractions was measured by ELISA kits (MyBioSource), according to the manufacturer's protocol.

Vessel Leakiness Assessment

Leaky blood vessels were histologically assessed upon intravenous injection of 10 kDa biotin-conjugated dextran (Molecular Probes). After 1 h, mice were perfused by intracardiac injection of saline for 5 minutes. Tumors were harvested and fixed in 2% PFA overnight, followed by immunofluorescent stainings.

Whole-Mount Ear Skin Staining

Skin samples were excised from ears of Balb/c mice and fixed overnight in 4% PFA. Subsequently, the samples were washed 2 times in PBS and permaebilized in block solution (PBS, 1% BSA, 0,3% TritonX 100) for 2 h. Skin pieces were then incubated overnight with primary antibodies: rabbit anti-Podoplanin (DSHB), rat anti-F4/80 (Serotec) in the block solution. The following day, samples were washed 3 times in 50% block, stained with appropriate secondary antibodies for 2h at RT, washed 3 times in 50% block and mounted on glass slides with Fluoromount G (Southern Biotech).

QUANTIFICATION AND STATISTICAL ANALYSIS

Data entry and all analyses were performed in a blinded fashion. All statistical analyses were performed using GraphPad Prism software on mean values, calculated from the averages of technical replicates. Statistical significance was calculated by two-tailed unpaired t-test on two experimental conditions or two-way ANOVA when repeated measures were compared, with $p < 0,05$ considered statistically significant. Detection of mathematical outliers was performed using the Grubbs' test in GraphPad. Sample sizes for all experiments were chosen based on previous experience and material availability. Independent experiments were pooled and analyzed together whenever possible as detailed in figure legends. All graphs show mean values ± standard error of the mean (SEM).

DATA AND CODE AVAILABILITY

The RNA sequencing data reported in this paper are deposited in the GEO database under the accession number GEO: GSE126722.